The Dissertation Committee for Seonpil Jang Certifies that this is the approved version of the following dissertation:

Inkjet Printed Single-Walled Carbon Nanotube Field Effect Transistors

Committee:

Ananth Dodabalapur, Supervisor

Deji Akinwande

Ray Chen

Paul Ho

Guihua Yu

Inkjet Printed Single-Walled Carbon Nanotube Field-Effect Transistors

by

Seonpil Jang, B.E.; M.E.

Dissertation

Presented to the Faculty of the Graduate School of

The University of Texas at Austin

in Partial Fulfillment

of the Requirements

for the Degree of

Doctor of Philosophy

The University of Texas at Austin

May 2016

Dedication

To my beloved father Gunho Jang, mother Heeyoung yang and wife Dr. Hyang Jee

Acknowledgements

Above all, I would like to thank my supervisor, Professor Ananth Dodabalapur, for his constant support and guidance over the past five years. His invaluable advice and encouragement on my work has been greatly appreciated. I would also like to thank my dissertation committee, Professor Deji Akinwande, Professor Ray T. Chen, Professor Paul S. Ho and Professor Guihua Yu for their helpful suggestions and advice on my dissertation. I would like to thank all of the present and former members of Dodabalapur research group: Dr. Taeho Jung, Dr. Byungwook Yoo, Dr. Yeontaek Jeong, Dr. Suvid Nadkarni, Dr. Chenguan Lee, Dr. Christopher Lombardo, Dr. Davianne Duarte, Dr. Leander Schulz, Dr. Tae-Jun Ha, Dr. Eric Danielson, Dr. Bongjun Kim, Rohit Yadav, Oleksiy Slobodyan, Barrett Worley, Seohee Kim, Xin Xu, Kelly Liang, and Michael Rodder for useful discussions, brainstorming, and helps in the lab. Particularly, I appreciate Dr. Yeontaek Jeong and Dr. Christopher Lombardo for the encouragement to initiate my Ph.D study at UT-Austin. I would also like to thank Oleksiy Slobodyan for his invaluable assistance in my writings and presentations. Thanks goes out to the Microelectronics Research Center staff, especially Ms. Jo Ann Smith, for all of their support. I would like to thank Professor Mark Hersam, Michael Geier, and Dr. Pradyumna Prabhumirashi at Northwestern University for their supply of valuable material and helpful discussions on my papers. I would also like to thank Kyunghwan Kim for helpful discussions on fabrications and his great sense of art in Sketch-Up.

I would like to thank my mother, father, and my brother for their love and support throughout the years. Lastly, I would like to thank my wife, Dr. Hyang Jee, for the great love and ultimate patient throughout my entire life, particularly Ph.D. student life.

Inkjet Printed Single-Walled Carbon Nanotube Field Effect Transistors

Seonpil Jang, Ph.D.

The University of Texas at Austin, 2016

Supervisor: Ananth Dodabalapur

Inkjet printing technology has the potential to drastically reduce the process time and cost by generating the patterns without physical masks and conventional vacuum processes. In addition, the inkjet printing process can be applied to flexible and large area substrates. Among the printable semiconductors, single walled carbon nanotubes (SWCNTs) have been attracting increasing attention for their high carrier mobility and potential application in transparent, flexible, high- current and high frequency electronics.

The effects of fluoropolymer capping onto SWCNT devices are investigated. Remarkable improvements in key device characteristics of SWCNT field-effect transistors (FETs) are achieved by coating of the active semiconductor with a fluoropolymer layer such as poly(vinylidene fluoride-trifluoroethylene) (P(VDF-TrFE)). These favorable changes in device characteristics also enhance circuit performance. The origins of these improvements are the dipolar nature of the fluoropolymer and the mechanism is confirm by exposing SWCNT FETs to a number of vapor phase polar molecules which produce similar effects on the FET characteristics as the application of P(VDF-TrFE).

High-performance inkjet printed single walled carbon nanotube (SWCNT) field effect transistors (FETs) with channel lengths of 150-250 nm are demonstrated. Optimized electrode geometry has been developed to confine the inkjet droplet to the active channel area. This minimizes waste of material outside of the channel while enabling short channel length devices that exhibit high effective carrier mobilities and transconductances. This novel fabrication approach is compatible with roll-to-roll processing and enables the formation of high-performance short channel device arrays based on inkjet printing with at least a 50-fold reduction in consumption of semiconducting SWCNT ink compared to other solution processing methods.

In these short channel SWCNT FETs, the influences of nanotube bending and gate insulator-semiconductor interface modification on the characteristics of inkjet printed short channel length SWCNT are investigated. Employing recessed source and drain (S/D) electrodes to minimize the mechanical distortion of CNTs, high performance short channel ambipolar transistors based on inkjet printed SWCNTs are demonstrated. Mechanical distortion of the nanotubes due to bending near source and drain contacts when they are not recessed is found to suppress electron transport and transform the ambipolar transistors into p-type devices. Inclusion of interfacial polymer layers such as P(VDF-TrFE) between the SWCNTs and Al_2O_3 top dielectric also results in p-type doping and reductions in electron transport transforming amibipolar transistors into p-type devices.

Table of Contents

List of Tables x

List of Figures xi

Chapter 1. Introduction 1

1.1. Printing Technologies 2

1.1.1. Contact printing technologies 2

1.1.2. Inkjet printing technologies 4

1.2. Inkjet Printing of Single-Walled Carbon Nanotubes 9

1.2.1. Single-walled carbon nanotubes 9

1.2.2. Carbon nanotube ink for inkjet printing 10

1.3. Organization of Dissertation 13

Chapter 2. Fluoropolymer Coating on Inkjet Printed Carbon Nanotube Transistors 15

2.1. Introduction 15

2.2. Experimental 17

2.2.1. Transistor device fabrication 17

2.2.2. Fluoropolymer capping on SWCNT FETs 18

2.3. Results and discussion 19

2.3.1. Device characteristics 19

2.3.2. Gate bias stability 21

2.3.3. Origin of improvements in fluoropolymer capping 23

2.3.4. Circuit characteristics with fluoropolymer capping 26

2.4. Conclusion 28

Chapter 3. Inkjet Printed Short Channel Carbon Nanotube Field Effect Transistors 29

3.1. Introduction 29

3.2. Experimental 31

3.2.1. Bottom-gate/top-contact structure 31

3.2.2. Top-gate/bottom-contact structure 37

3.2.3. Electron beam lithography 39
3.3. Results and discussion 40
3.3.1. Material consumption of solution processing methods. 40
3.3.2. Bottom-gate/top-contact structure 41
3.3.3. Top-gate/bottom-contact structure 43
3.4. Conclusion 47

Chapter 4. Short Channel Ambipolar Transistors with Inkjet Printed Semiconducting Carbon Nanotubes 49
4.1. Introduction 49
4.2. Experimental 51
4.2.1. Device fabrication 51
4.2.2. Electrical characterization of devices 52
4.3. Results and discussion 52
4.3.1. Conventional short channel SWCNT FETs 52
4.3.2. Short channel SWCNT FETs with recessed S/D electrodes 55
4.3.3. Electrical characteristics of short channel ambipolar SWCNT FETs 56
4.3.4. Gate insulator interface modification by fluoropolymer 59
4.4 Conclusion 61

Chapter 5. Conclusion 62

Appendix 64

References 66

Vita 73

List of Tables

Table 3.1: Required volume of solution and estimated weight of SWCNTs for common solution-processing methods.....40

Table 3.2: Comparison on the performance of inkjet / aeosol-jet printed SWCNT FETs.....48

List of Figures

Figure 1.1: Schematic illustrations of contact printing of nanowire-based integrated devices. (a) Dry-transfer printing. (b) Microcontact printing. (c) Direct contact printing. (d) Direct transfer printing. Reproduced from Ref. 28 with permission from The Royal Society of Chemistry. 3

Figure 1.2: Schematic of a continuous inkjet (CIJ) printer.....4

Figure 1.3: Schematics of drop-on-demand mode inkjet printing (a) piezoelectric inkjet printing and (b) thermal inkjet printing. 6

Figure 1.4: The schematic of a piezoelectric nozzle chamber showing the waveforms and their corresponding PZT deflection.....8

Figure 1.5: Single-walled carbon nanotube (SWCNT) (a) Illustration of SWCNT and (b) Electron microscopy of SWCNTs. (b): Reprinted by permission from Macmillan Publishers Ltd.: Nature (Ref. 37), copyright (1993)10

Figure 1.6: Photograph and illustration of SWCNTs after separation in various color bands. Reprinted with permission from (M. S. Arnold, S. I. Stupp, and M. C. Hersam, "Enrichment of Single-Walled Carbon Nanotubes by Diameter in Density Gradients," *Nano Letters,* vol. 5, pp. 713-718, 2005). Copyright (2005) American Chemical Society 11

Figure 2.1: Schematic cross-section of inkjet printed SWCNT FETs with bottom-gate/bottom-contact structure.....17

Figure 2.2: Schematic illustration of fluoropolymer (P(VDF-TrFE)) capping process.....18

Figure 2.3: Electrical characteristics of SWCNT FETs with spin coated P(VDF-TrFE) on top of the active semiconductor layer. (a) and (b) are I_D-V_{GS} curves of SWCNT FETs before and after P(VDF-TrFE) spin-coating, respectively (Insets show the device structures). (c) On/Off current ratio before and after P(VDF-TrFE) spin-coating. (d) Effect of spin-coated P(VDF-TrFE) on threshold voltage (V_{th}) distributions of SWCNT FETs. The box chart indicates the average of V_{th} (solid square), minimum and maximum values (cross), and the range from 25% to 75% (box). ...19

Figure 2.4: Electrical characteristics of SWCNT FETs with inkjet printed P(VDF-TrFE) on top of the semiconductor layer. (a) and (b) are double swept I_D-V_{GS} curves of SWCNT FETs before and after P(VDF-TrFE) inkjet printing, respectively. (c) On/Off current ratio before and after P(VDF-TrFE) inkjet printing. (d) Effect of inkjet printed P(VDF-TrFE) on the hysteresis of SWCNT FETs. The box chart indicates the average of V_{th} (solid square), minimum and maximum values (cross), and the range from 25% to 75% (box). 20

Figure 2.5: Transfer characteristics during the gate bias stress on SWCNT FETs with and without inkjet printed P(VDF-TrFE) cap layer. (a) and (b) are positive gate bias stress on SWCNT FETs with and without inkjet printed P(VDF-TrFE) cap layer, respectively. (c) and (d) are negative gate bias stress on SWCNT FETs with and without P(VDF-TrFE), respectively. 21

Figure 2.6: The passivation benefits of inkjet printed P(VDF-TrFE) on gate bias stress stability. Threshold voltage shift (ΔV_{th}) with stress time under (a) positive gate bias stress (PGBS) and (b) negative gate bias stress (NGBS). The magnitude of the gate bias was fixed at ± 5V (1.85 MV/cm), and V_{DS} was fixed at -1 V. 22

Figure 2.7: Experimental set-up for vapor exposure test of SWCNT FETs. 24

Figure 2.8: Vapor phase organic solvent exposure test on a SWCNT FET. Transfer characteristics were measured prior to, during, and after the vapor flow on the SWCNT FET; (a) acetone, (b) ethanol and (c) hexane. (d) On-state current (solid symbols) and off-state current (open symbols) extracted from transfer curves were compared. 25

Figure 2.9: Transfer characteristics of the SWCNT FETs with various annealing temperatures of P(VDF-TrFE). (a) double-swept transfer curves starting from V_{GS}=4V showing the gate hysteresis. (b) single-swept transfer curves starting from V_{GS}=4V. 26

Figure 2.10: (a) Circuit diagram of a five-stage ring oscillator. (b) The output signal of a five-stage ring oscillator based on SWCNTs and ZTO complementary circuit with spin coated PVDF. 27

Figure 3.1: Device configurations for short channel SWCNT FETs. (a) Bottom-gate/top-contact. (b) Top-gate/bottom-contact 30

Figure 3.2: Schematic illustrations and images showing the process flow for inkjet printed SWCNT FET with bottom-gate/top-contact device structure. (a) Single drop inkjet printing of the SWCNT ink onto ZrO_2 dielectric. (Inset) Optical image of the inkjet printed droplet (10 pL). (b) SEM image to confirm the exact location of printed SWCNTs. (c) Electron beam lithography process to pattern S/D electrodes onto printed SWCNTs. (inset) SEM image showing the completed device (red square).....32

Figure 3.3: Optical images of 10 pL inkjet printed droplets of SWCNT ink (a) on UV O_3 treated substrate at 21^oC printing plate temperature, (b) on untreated substrate at 21^oC printing plate temperature, (c) on UV O_3 treated substrate at 60^oC printing plate temperature, (d) on untreated substrate at 60^oC printing plate temperature.....33

Figure 3.4: Scanning electron microscope (SEM) images of 10 pL inkjet printed droplets of SWCNT ink (0.1 mg mL^{-1}) (a) on UV O_3 treated substrate at 21^oC printing plate temperature, (b) on untreated substrate at 21^oC printing plate temperature, (c) on UV O_3 treated substrate at 60^oC printing plate temperature, (d) on untreated substrate at 60^oC printing plate temperature. Areas of SWCNTs are outlined with red lines....34

Figure 3.5: Surface energy analysis of ZrO_2 substrates. (a) Contact angle measurement of various ZrO_2 substrates using deionized water and ethylene glycol. (b) Calculated surface energy based on contact angle measurements.....36

Figure 3.6: A schematic illustration of the process flow for inkjet printed a SWCNT FET with top-gate/bottom-contact device structure. (a) Electron beam lithography (EBL) is used to pattern S/D electrodes on the Al_2O_3 substrate. (b) Single drop (10 pL) inkjet printing of SWCNTs on the prepatterned S/D area. (c) Deposition of top dielectric, 30 nm thick Al_2O_3, by ALD and top gate electrode patterned by EBL. (d) Wet etching process with hydrofluoric acid to form via holes for probe contact pads.....37

Figure 3.7: Electrical characteristics of inkjet printed SWCNT FETs with bottom-gate/top-contact device structure (L_{ch} = 250 nm). (a) Measured I_d-V_g transfer characteristics of UV O_3 treated (red squares) and untreated (black squares) SWCNT FETs. (b) Measured I_d-V_d output characteristics of UV O_3 treated SWCNT FETs.....41

Figure 3.8: SEM images showing the difference in concentration of SWCNTs according to UV O_3 treatment: (a) with UV O_3 treatment, (b) without UV O_3 treatment. 42

Figure 3.9: SEM image of the bottom-gate/top-contact device. Approximately 30 individual SWCNTs connect the S/D electrodes (L_{ch} = 250 nm).....43

Figure 3.10: (a) Optical image of the inkjet printed droplets demonstrating droplet confinement by the prepatterned rectangular metal line structure. The diameter of the droplet without confinement on Al_2O_3 is 160 μm (red square), and is larger than the confinement area of 60 μm × 60 μm (red arrow). (b) Scanning electron microscope (SEM) image of an inkjet printed droplet confined within the rectangular area within which the S/D electrodes were prepatterned. (c) SEM image of SWCNTs extending between S/D electrodes. (d) Optical image of inkjet printed SWCNT FETs with top-gate/bottom-contact device structure. 43

Figure 3.11: Electrical characteristics of inkjet printed SWCNT FETs with top-gate/bottom-contact device structure. (a) Measured I_d-V_g transfer characteristics (blue lines) and normalized transconductance g_m (red squares) for a 190 nm device. (b) Measured I_d-V_d output characteristics of a 190 nm device. (c) Measured I_d-V_g transfer characteristics (blue squares) and diameter-normalized current (red line) of a 150 nm device. 46

Figure 4.1: (a) Schematic illustration of the process flow for inkjet printed SWCNT FETs with top-gate/bottom-contact device structure. (b) Measured I_D-V_{GS} transfer characteristics of 190 nm channel length device showing the difference between bottom-gate operation (black squares) and top-gate operation (red circles). (c) Measured I_D-V_{DS} output characteristics of the 190 nm channel length device. The red circle indicates weak ambipolar characteristics. (d) SEM image showing the bending of CNTs due to surface relief of the S/D contacts. (inset) Schematic illustration of the top-gate/bottom-contact device structure with raised S/D electrodes.53

Figure 4.2: (a) A schematic illustration of a completed device of top-gate/bottom-contact structure with typical raised S/D electrodes. AFM image and step profile of stacked S/D electrodes. (b) A schematic illustration of a completed device of top-gate/bottom-contact structure with flattened S/D electrodes. AFM image and step profile of flattened S/D electrodes. 55

Figure 4.3: Electrical characteristics of top-gate/bottom-contact device with flattened S/D electrodes. (a) I_D-V_G transfer characteristics of device with channel length 200nm showing balanced ambipolar characteristic with 10 SWCNTs (blue hexagons are transconductance per SWCNT). (b) I_D-V_D output characteristics of device with channel length of 200nm. .57

Figure 4.4: (a) Comparison of I_D-V_G transfer characteristics between measurments in air and vacuum (1×10^{-3} Torr) for a top-gate/bottom contact device with recessed S/D electrodes. (b) Shelf life of a top-gate/bottom contact device with recessed S/D electrodes stored in air. 58

Figure 4.5: (a) Electrical characteristics of a top-gate/bottom contact device with flattened S/D electrodes and inkjet printed P(VDF-TrFE) (L_{ch} = 200 nm). (b) Statistical data of the p-branch and n-branch on-current levels for various device structures (10 devices for each structure). 60

Chapter 1. Introduction

Recently, diverse research on solution based processes has attracted tremendous interest in the electronics field as a complement to conventional fabrication technologies. Solution based processes are cost effective: reducing material usage and eliminating expensive vacuum deposition steps, and also applicable to novel printing processes such as roll-to-roll printing or inkjet printing. There has been a great deal of research on developing thin-film transistors (TFTs) suitable for printed electronics. Impressive improvements in the performance characteristics of semiconducting polymer [1, 2], organic semiconductor [3-5], semiconducting single walled carbon nanotube (SWCNT) [6-10], and amorphous metal oxide semiconductor [11-13] based transistors and in implementing circuits based on them have been made [14-17].

SWCNT field effect transistors (FETs) have been extensively investigated for use in nanoelectronic devices because of their high carrier mobility and potential applications in transparent and flexible electronics [18-20]. Recent advances in the availability of SWCNT source material with > 98% semiconducting nanotubes [21-23] and in printing such nanotubes to realize high-performance FETs make them very promising candidates for printed electronics. In addition, SWCNT networks exhibit excellent mechanical flexibility owing to their inherently small diameters [24]. These outstanding electrical and mechanical properties of SWCNTs may offer solutions for realization of high performance and highly bendable FETs in the emerging flexible electronics field.

The purpose of this dissertation is to investigate inkjet printed SWCNTs, one of the most attractive printable semiconducting materials, and improve the characteristics of inkjet printed SWCNT FETs which have conventional micron-scale channel lengths. In addition, scaling down of inkjet printed SWCNT FETs is also investigated.

1.1. PRINTING TECHNOLOGIES

Printing technologies have been industrialized and have served an essential part of publishing and transaction printing for a century. In recent years, printing techniques have been utilized to directly deposit electronic materials on a substrate in order to build electronic devices such as passive resistors, capacitors, inductors, and active transistors [25, 26]. Conventional fabrication processes used extensively in electronic devices consist of a series of thin film deposition steps using vacuum processing, along with a series of lithography processes that include photoresist deposition, exposure, development, etching and photoresist stripping in order to define the thin film into a desired pattern. This subtractive patterning method wastes the etched materials as well as several layers of costly masks, increasing the total processing cost and time. On the other hand, printing processes such as contact printing and inkjet printing additively deposit materials into a predesigned pattern. The advantage of combining thin film deposition and patterning into a single step eliminates the major cost points encountered in conventional vacuum and lithographic processing [15, 26, 27].

1.1.1. Contact printing technologies

Conventional printing consists of offset, flexography, gravure and screen printing technologies, in which the image/pattern is transferred to substrates from prefabricated plates, cylinders or screens. High throughput products such as newspapers, books, and magazines are made using conventional printing methods. Printed electronics may begin to exploit high-throughput roll-to-roll processing similar to that of the publishing industry. Roll-printing processes have been demonstrated to print circuits as fast as five

meters per minute, a speed quite capable of competing with parallel vacuum deposition processes [25]. Roll-to-roll printing can be applied to flexible substrates such as plastic or paper for realizing flexible electronics. Figure 1.1 shows some examples of contact printing which have been utilized in the microelectronics field [28].

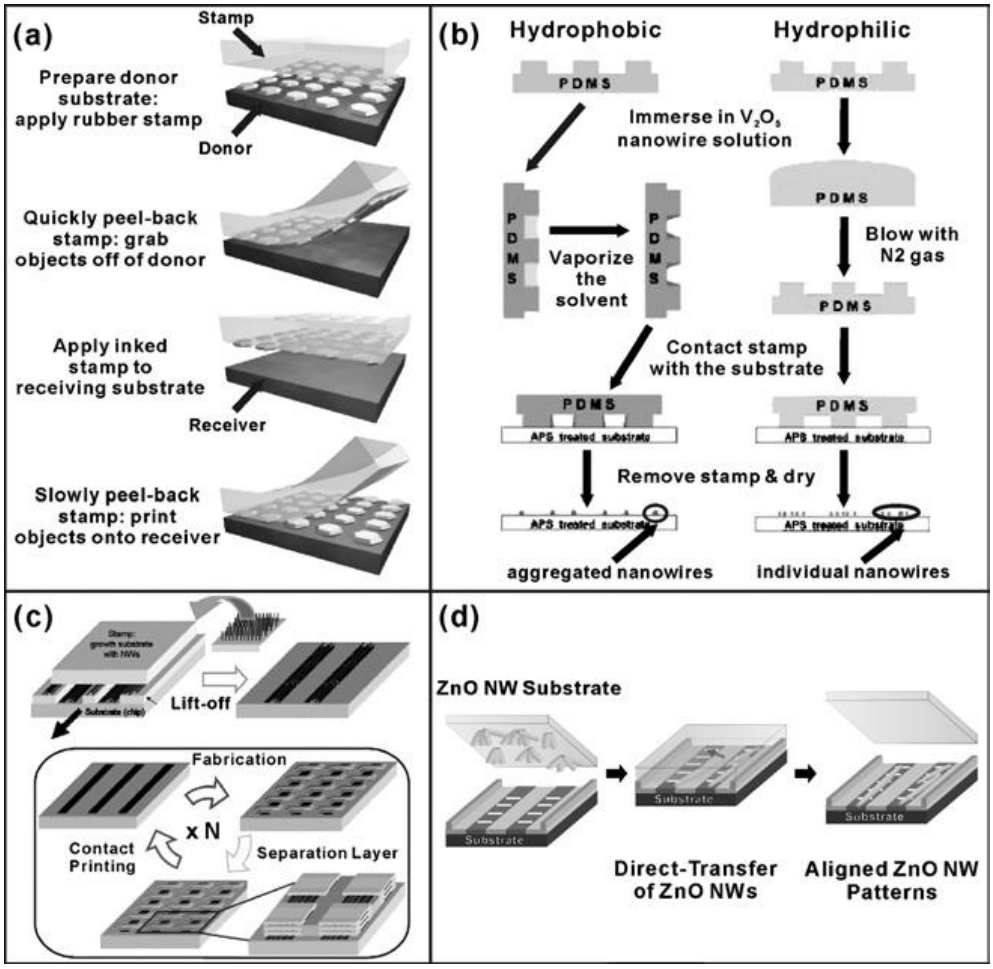

Figure 1.1: Schematic illustrations of contact printing of nanowire-based integrated devices. (a) Dry-transfer printing. (b) Microcontact printing. (c) Direct contact printing. (d) Direct transfer printing. Reproduced from Ref. 28 with permission from The Royal Society of Chemistry.

1.1.2. Inkjet printing technologies

Inkjet printing technology can be described as a technique in which an extremely repeatable formation of small fluid droplets is directed to a specific location with high accuracy. Inkjet printing technology can be divided into two categories: continuous mode and drop-on-demand (DoD) mode. In the continuous mode, ink is continuously jetted and the charged ink droplets are guided by deflection plates onto the substrate [29]. Figure 1.2 shows the continuous type inkjet printing system.

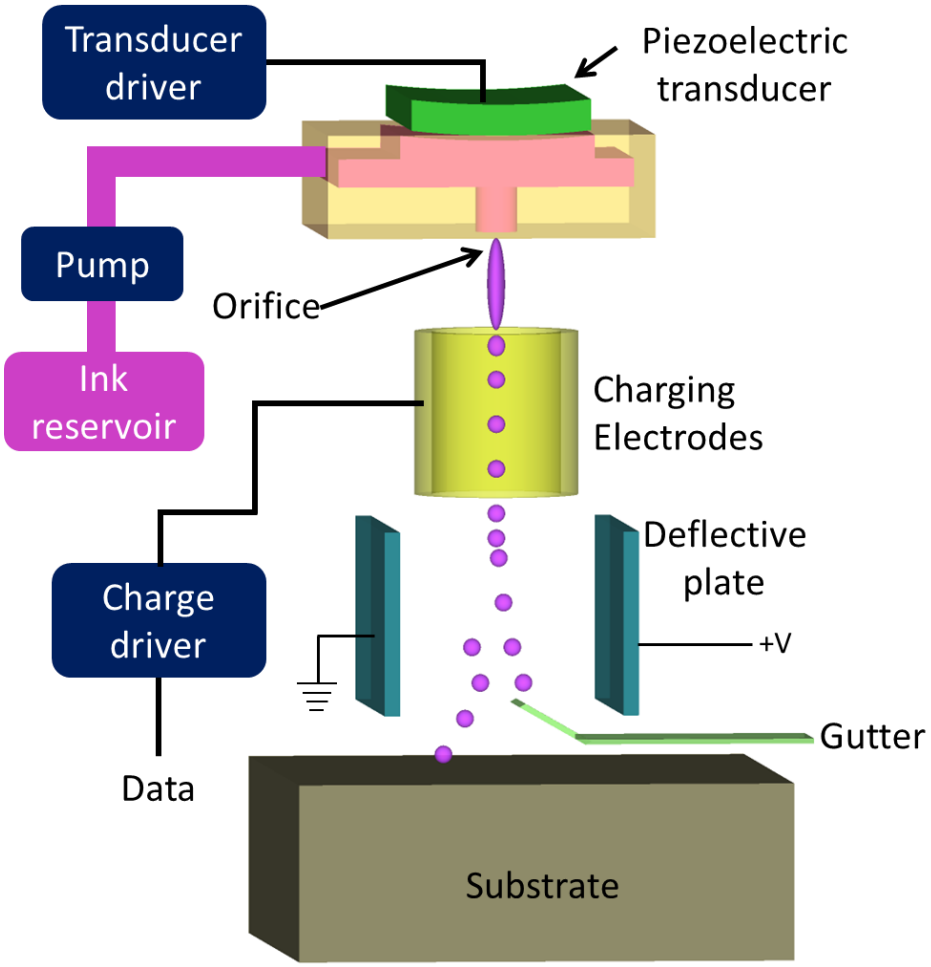

Figure 1.2: Schematic of a continuous inkjet (CIJ) printer.

DoD inkjet mode uses computer-aided design image file and provides high speed and scalability, allowing the use of multiple nozzles operated in high-frequency. DoD inkjet processes can be classified according to the way that the individual drop is generated: piezoelectric or thermal inkjet printing. In DoD mode, a small transducer is used to displace ink by creating a pressure wave which travels to an orifice or nozzle and ejects a droplet. In piezoelectric inkjet printers the pressure is generated by piezoelectric actuators, while in thermal inkjet printers a heating element evaporates a small amount of solvent resulting in vapor generation and volume expansion, hence displacement and ejection of the ink [30-32]. Figure 1.3 describes the generic working mechanism for piezoelectric (a) and thermal (b) printing heads [32].

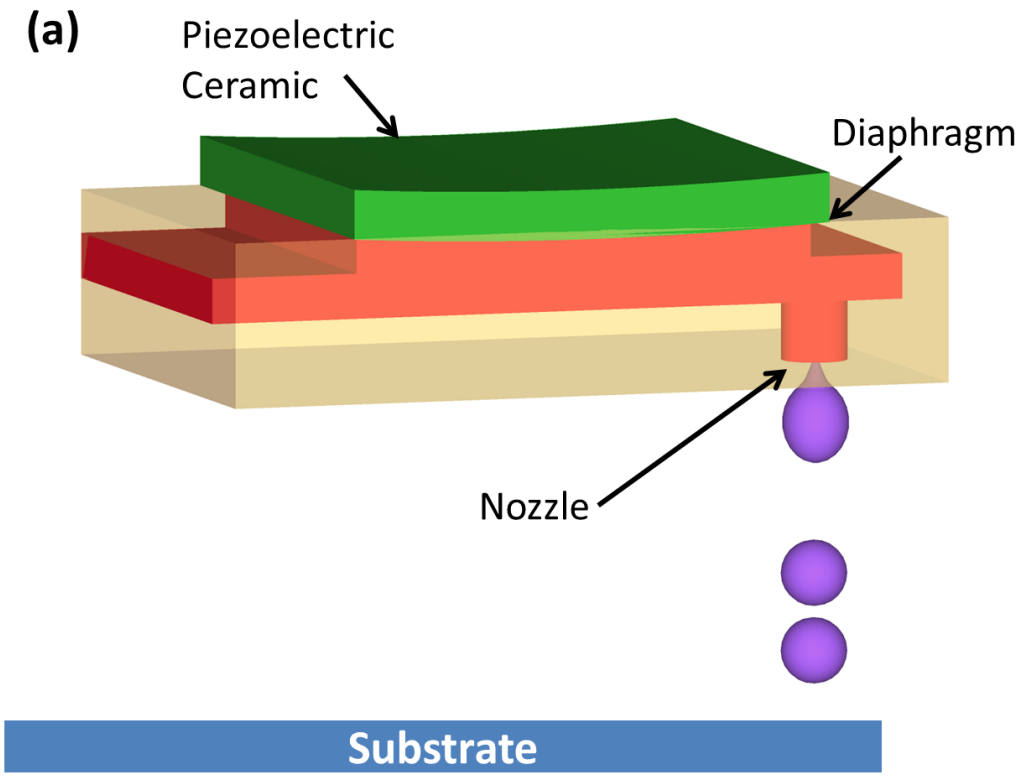

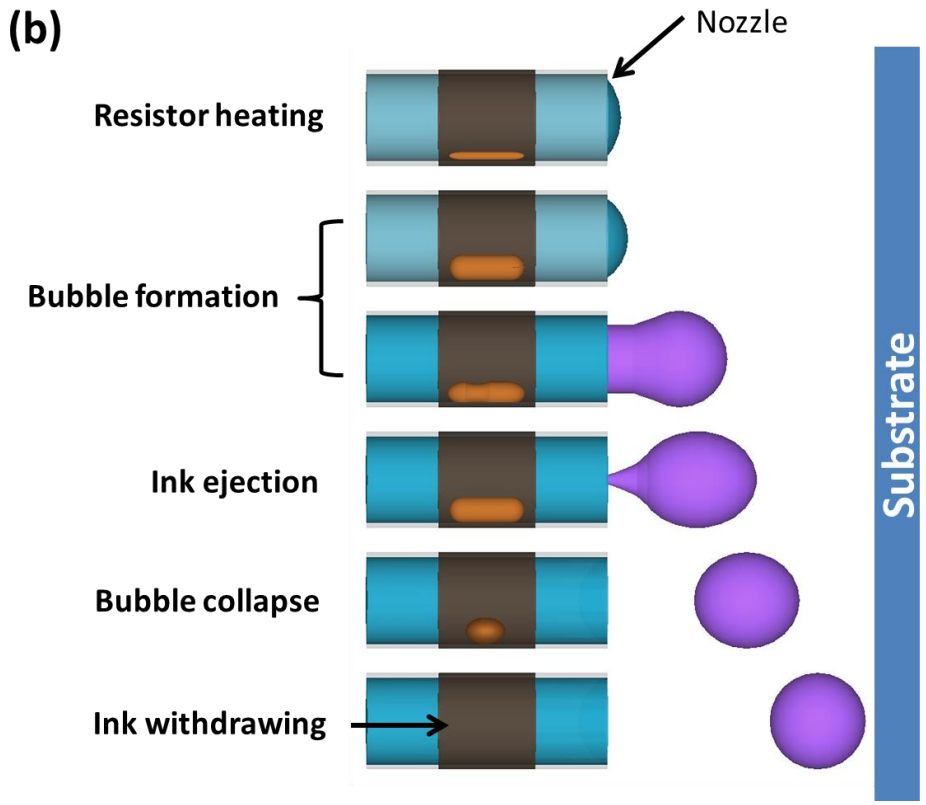

Figure 1.3: Schematics of drop-on-demand mode inkjet printing (a) piezoelectric inkjet printing and (b) thermal inkjet printing.

Due to the low cost of thermal-bubble jet nozzle, majority of the consumer inkjet printers available today utilize thermal-bubble technology. However, piezoelectric inkjet is more preferable for the microelectronic field, because thermal-bubble jet has several disadvantages. The nozzles typically suffer from a short lifetime due to residue build-up on the heating element. Moreover, special ink is required to resist rapid thermal change. For these reasons, thermal-bubble jets may not suitable for printing electronic devices, as the inks used are not compatible with the sudden heat change, e.g. metal nanoparticles can be sintered due to the heat, resulting in deposition of metal layers on the heating elements.

The jetting in the piezoelectric nozzle is controlled by a waveform applied to the piezoelectric plate. For the Dimatix system (FUJIFILM Dimatix, Inc.), a widely used material inkjet printer for printed electronics research, the ink reservoir is fabricated using silicon MEMS processes to create an internal chamber and a membrane designed to be deflected by a piezoelectric material, Lead Zirconate Ttitanate (PZT). As illustrated in Figure 1.4, droplet formation is driven by a waveform that can be divided into four segments. The amplitude and the slew rate of the waveform determine the amount and the rate of the PZT deflection respectively [33]. In the first phase, voltage is decreased to retract the PZT to draw fluid into the pumping chamber, followed by a settling time. This section creates two in phase acoustic waves that propagate from both ends of the chamber through the inlet and travel in opposite directions. Phase two of the waveform is the drop ejection phase. When voltage is increased, PZT expands precisely resulting in compressing the chamber and generating pressure to eject a drop [34, 35]. Higher droplet energy can be also achieved by using a steeper slope or higher voltage in phase two, resulting in a faster PZT deflection. At phase three, the PZT retracts slightly from phase two to break the droplet from the chamber. The intermediate voltage in phase three also provides a damping effect to prevent air from being sucked back into the chamber. Finally, the voltage returns back to the standby state in phase four filling the small amount of ink into the chamber.

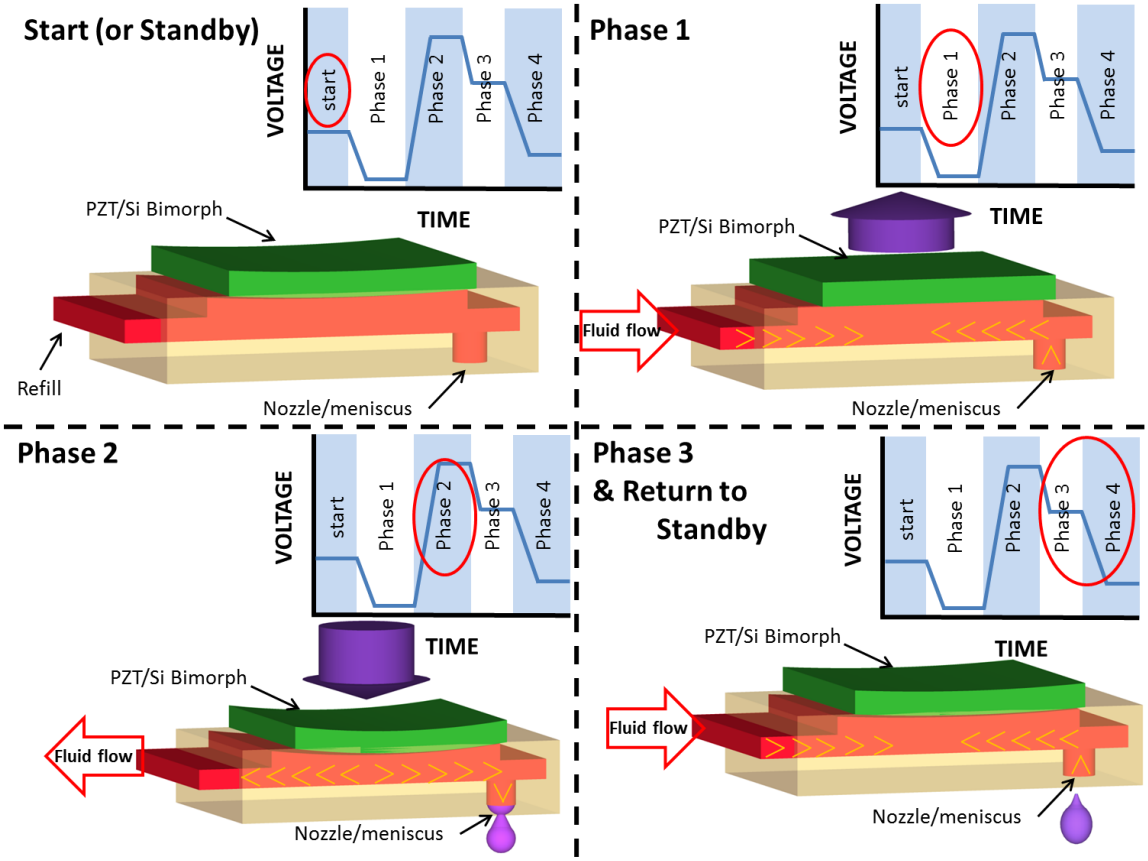

Figure 1.4: The schematic of a piezoelectric nozzle chamber showing the waveforms and their corresponding PZT deflection.

1.2. INKJET PRINTING OF SINGLE-WALLED CARBON NANOTUBES

As discussed earlier, inkjet printing technology has been attracting extensive interest due to its additive and contact-less processing. In addition, the flexibility of pattern adjustment and elimination of a physical mask have significantly reduced the research time and cost required from idea to proof-of-concept demonstration. Therefore, there has been increasing research studying passive and active printed devices using inkjet exclusively [4, 26, 36]. In this dissertation, piezoelectric type DoD inkjet printing technique has been studied and employed to deposit semiconducting single-walled carbon nanotubes (SWCNTs) forming active layer.

1.2.1. Single-walled carbon nanotubes

In 1993, a Japanese research group led by Professor Sumio Iijima reported their discovery and proof of a new kind of nanostructured materials: single-walled carbon nanotubes (SWCNTs) [37]. As shown in Figure 1.5, an SWCNT can be represented a long and thin cylinder (with a diameter typically about 1 nm) of carbon atoms each sitting on one of the six corners of a honeycomb hexagon connected by the strong chemical bonds through the so-called sp^2 hybridization. SWCNT can also be thought of as a ribbon of graphene rolled into a seamless, one-atom thick cylinder. Such a unique quasi one-dimensional structure produces a range of intriguing properties. In particular, SWCNTs are mechanically strong, flexible, and can be either electrically conductive or semiconducting [38].

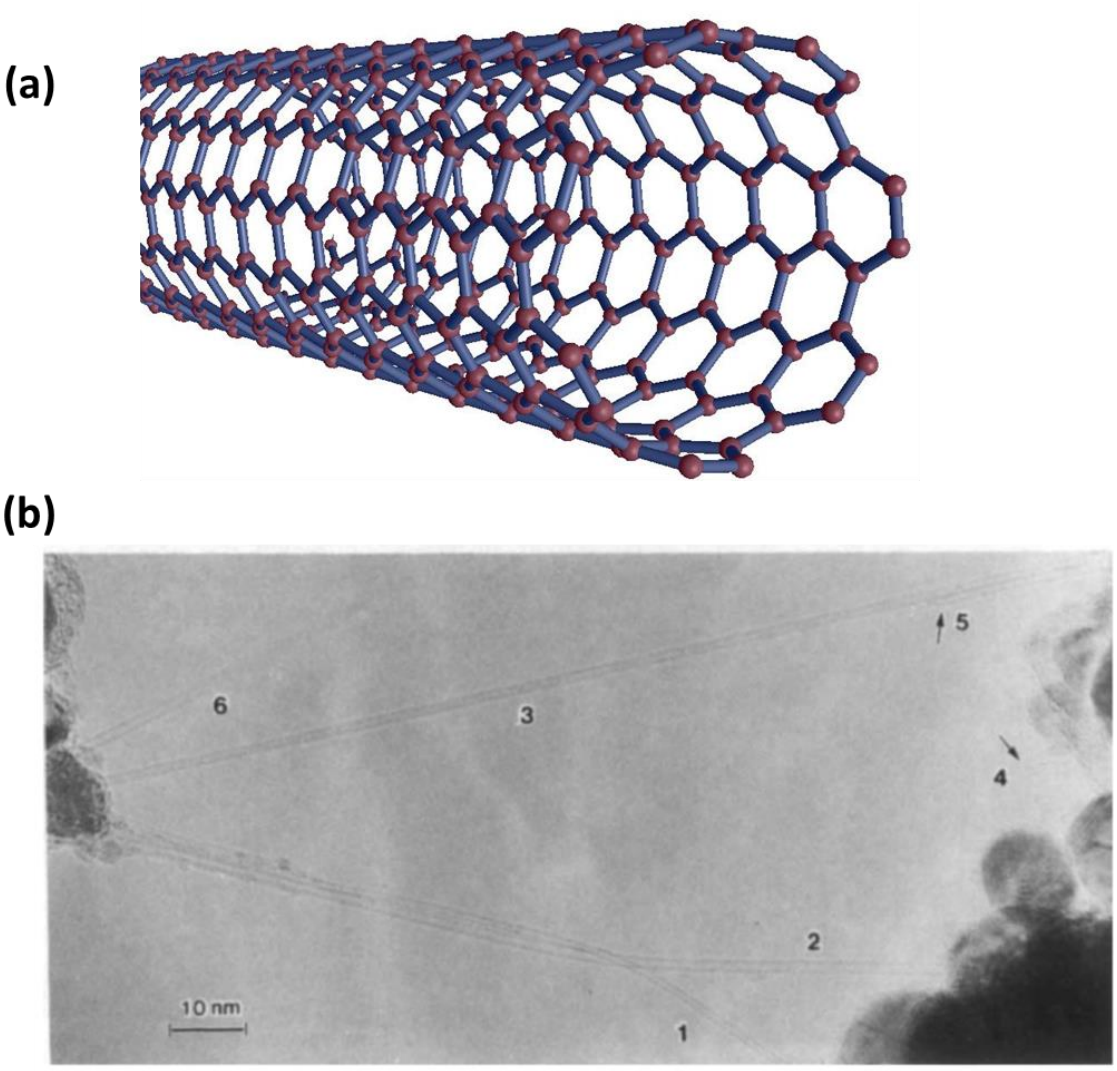

Figure 1.5: Single-walled carbon nanotube (SWCNT) (a) Illustration of SWCNT and (b) Electron microscopy of SWCNTs. (b): Reprinted by permission from Macmillan Publishers Ltd.: Nature (Ref. 37), copyright (1993)

1.2.2. Carbon nanotube ink for inkjet printing

In 2005, research group led by Dr. Mark C. Hersam achieved the bulk enrichment and separation of DNA-wrapped SWCNTs by nanotube diameter using density-gradient

ultracentrifugation (DGU) [39], which has been commonly used to separate and isolate biological macromolecules. As shown in Figure 1.6, the enrichment of semiconducting SWCNTs by diameter was achieved using density gradients in aqueous solutions of iodixanol, and isolated SWCNTs separated into colored band in the density gradient during centrifugation.

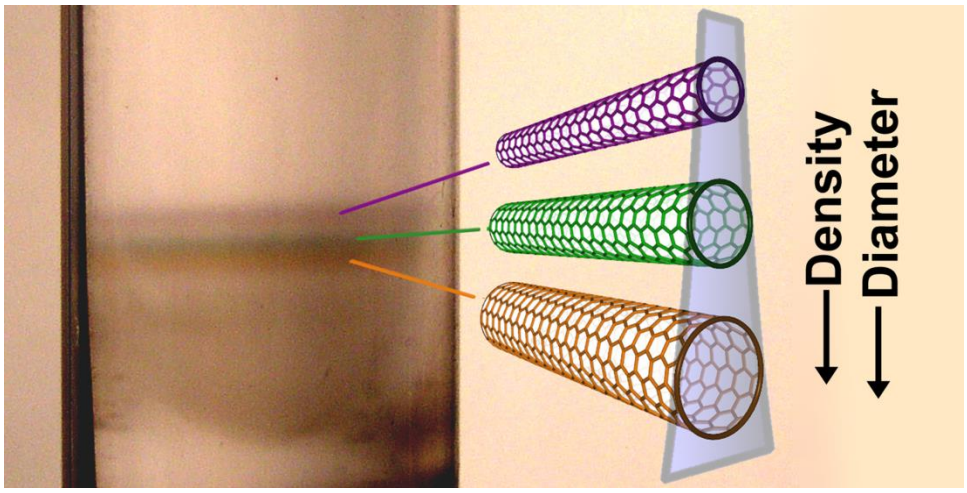

Figure 1.6: Photograph and illustration of SWCNTs after separation in various color bands. Reprinted with permission from (M. S. Arnold, S. I. Stupp, and M. C. Hersam, "Enrichment of Single-Walled Carbon Nanotubes by Diameter in Density Gradients," *Nano Letters,* vol. 5, pp. 713-718, 2005). Copyright (2005) American Chemical Society

This technique was expanded into sorting of SWCNTs by band gap and electronic type using structure-discriminating surfactants [21]. A chirality-based sorting methods also developed based on this DGU technique [22].

SWCNTs used in this dissertation were highly sorted semiconducting SWCNTs (>98%) using DGU and provided by Dr. Hersam's groupt at Northwestern University. These sorted semiconducting SWCNTs should be dispersed uniformly in the solvent to

achieve printable solution. SWCNTs can be dispersed in aqueous solutions and organic solvents. There are several advanced skills in the literatures for preparation of SWCNT solutions or suspensions especially in the aqueous solvents. However, in order to achieve optimal performance of the printer and produce reliable printed patterns, the inks should possess proper fluidic characteristics, including viscosity and surface tension [33, 40].

The quality of printable water-based SWCNT solution (ink) plays a key role in fabricating high-performance TFTs. In order to evaluate the inks, Jianwen Zao, et al. [41] synthesized SWCNTs and made functionalized SWCNT inks. Various inks were first printed on SiO_2/Si substrates with pre-patterned gold electrodes by inkjet printing and the electrical properties of the printed TFTs were then measured.

According to their report, surfactant concentration is critical because the hydrophobic surface of the nanotubes needs to be changed to hydrophilic by attaching polar chemical groups that interact and form hydrogen bonds with water molecules. Moreover, the performance of the printing and the electrical property of the printed devices are strongly influenced by the concentration of PVP in the inks. There should be sufficient PVP in the inks since PVP is an excellent additive for the SWCNT ink. Since PVP can increase the ink viscosity and debundle SWCNTs, it stabilizes the inks for a long time, and improve the printed device patterns. On the other hand, there should not be too much PVP in the inks since the ink with excessive PVP may be too viscosity and cannot drip out of the nozzles. In addition, PVP itself is insulating and too much PVP can severely degrade the conductance of the printed SWCNT TFTs.

This project was also started with aqueous SWCNT solutions. However, water based SWCNT ink caused severe clogging issues in our inkjet printing system, thus the solvent system for our SWCNT ink was changed to the organic solvent, 1-cyclohexyl-2-pyrrolidone (CHP), which has the highest dispersibility among the organic solvents [42].

Even though organic solvent system requires higher baking temperature than that of conventional aqueous solution, the printability and dispersibility of SWCNTs in CHP is superior to the SWCNT aqueous solution. In this dissertation, all the experiments of inkjet printed SWCNT FETs were performed using CHP based organic solvent system[43-45].

1.3. ORGANIZATION OF DISSERTATION

The purpose of this dissertation is to describe the development of high performance thin film transistors (TFTs) based on inkjet printed semiconducting single-walled carbon nanotubes (SWCNTs). The dimension of investigate devices is started from conventional micron-scale channel length and scaled down to 150 nm, in which the several individual SWCNTs span the entire source/drain (S/D) gap minimizing intertube junction of SWCNTs. In order to solve the mechanical distortion of SWCNTs in the short channel device, recessed S/D electrodes designs are employed and investigated. Development of new device structure, device fabrication, novel material and device characterizations are discussed.

This dissertation is divided into five chapters. Chapter 2 describes a development of surface treatment for inkjet printing of SWCNTs, and discusses fabrication process and characteristics of micron-scale SWCNT devices. It is shown that the use of coating of fluoropolymer results in substantial improvements in the characteristics of inkjet printed SWCNT FET devices and circuits.

Chapter 3 describes a method of inkjet printing submicron-scale SWCNT field effect transistors (FETs) with channel lengths of 150-200 nm. Novel electrode design for inkjet printing implies minimal consumption of SWCNT ink, thus realizing one of the

primary benefits of additive manufacturing. Two representative device structures for short channel SWCNT FETs are compared.

Chapter 4 illustrates short channel ambipolar FETs with inkjet printed semiconducting SWCNTs. The influence of nanotube bending and gate insulator-semiconductor interface on the characteristics of inkjet printed short channel SWCNT FETs is described. Balanced ambipolar transport characteristics of SWCNT devices are demonstrated and the effect of fluoropolymer interfacial layer is discussed.

Finally, Chapter 5 summarizes the conclusions drawn from this study and presents recommendations for future work.

Chapter 2. Fluoropolymer Coating on Inkjet Printed Carbon Nanotube Transistors*

2.1. INTRODUCTION

SWCNT FETs are intrinsically ambipolar [46-48]; however, trapping of electrons often results in the observation of only p-channel FET behavior when exposed to air [47, 49]. The threshold voltage of our printed SWCNT p-channel FETs is typically negative and the off-current value is high [27]. This prevents the FETs from turning off completely at V_{GS} = 0V, which complicates the design of enhancement mode circuits based on SWCNTs, resulting in high power dissipation and reduced noise margins and stability [50]. This has hitherto been one of the primary drawbacks of SWCNT FETs, thus limiting their implementation in printed electronics circuit and systems applications. Therefore, it is highly desirable to be able to reduce the magnitude of the threshold voltage, reduce the off-current, and decrease the device-to-device variations in threshold voltage, hysteresis, and related device metrics.

In this chapter, we report on a general method to achieve these objectives and demonstrate results with discrete devices and complementary ring oscillator circuits. We also report on the effects of exposing SWCNT FETs to vapors with different polarity (as characterized by the dipole moments) on SWCNT FET performance characteristics and find convincing evidence that polar species in contact with the SWCNTs can reduce the apparent background impurity concentration and device threshold voltage. We use

* This chapter is based on Reference 43: Jang, S.; Kim, B.; Geier, M. L.; Prabhumirashi, P. L.; Hersam, M. C.; Dodabalapur, A. Fluoropolymer Coating for Improved Carbon Nanotube Transistor Device and Circuit Performance. *Appl. Phys. Lett.,* **2014**, *105*, 122107. S.J. and A.D. designed the experiments. S.J. carried out fabrication and characterization of devices. B.K. helped with circuit experiment. P.L.P., M.L.G., and M.C.H. provided semiconducting SWCNTs.

these results to propose a model that describes the effects of fluoropolymer capping on SWCNT FET characteristics. Our research has been influenced by recent results from our group on the impact of fluoropolymer capping layers on the transport characteristics of monolayer graphene FETs [51]. Here, we report improvements in the transport characteristics and threshold voltage distribution in SWCNT FETs through the use of poly(vinylidene fluoride-trifluoroethylene) (P(VDF-TrFE)) capping layers.

2.2. EXPERIMENTAL

2.2.1. Transistor device fabrication

The schematic cross-section of a SWCNT FET fabricated by inkjet printing is illustrated in the inset in Figure 2.1. Heavily doped Si substrates were used as a global gate in the bottom gated, bottom-contact device configuration. A high-κ dielectric, ZrO_2, was deposited from solution by a sol-gel route. Source and drain (S/D) electrodes consisting of a Ti/Au (3 nm/35 nm) double layer were deposited by thermal evaporation followed by the lift-off process. After the deposition of S/D electrodes, the dielectric surface was treated by UV light in air for 10 minutes to modify its surface characteristics so as to achieve a spatially uniform network of CNTs upon inkjet printing. Highly enriched semiconducting SWCNTs (>98% purity, achieved by density gradient ultracentrifugation [21, 22] dispersed in 1-cyclohexyl-2-pyrrolidone (CHP) were inkjet printed on to the UV O_3 treated ZrO_2 substrate to form the channel layer.

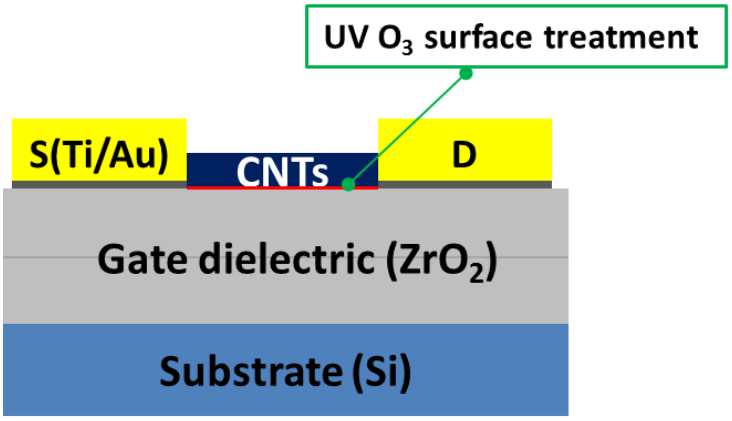

Figure 2.1: Schematic cross-section of inkjet printed SWCNT FETs with bottom-gate/bottom-contact structure.

2.2.2. Fluoropolymer capping on SWCNT FETs

After measuring the initial electrical characteristics of the inkjet printed SWCNT FETs, P(VDF-TrFE) films were deposited from diethyl carbonate solution by spin-coating or inkjet printing as illustrated in Figure 2.2. P(VDF-TrFE) copolymer powder with 30% molar ratio of TrFE (Solvay Inc.) was dissolved in diethyl carbonate. Two different solutions, having P(VDF-TrFE) concentrations of 2.5 and 0.5 weight to volume percent (% w/v) were prepared for spin-coating and inkjet printing, respectively. P(VDF-TrFE) films were annealed at 140°C for 3 minutes in air on a hot plate.

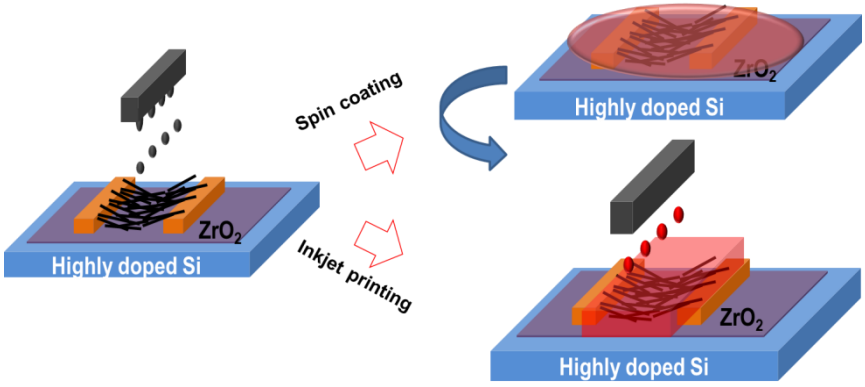

Figure 2.2: Schematic illustration of fluoropolymer (P(VDF-TrFE)) capping process.

2.3. RESULTS AND DISCUSSION

2.3.1. Device characteristics

The device characteristics before and after P(VDF-TrFE) spin-coating are compared in Figure 2.3. The use of the P(VDF-TrFE) cap layer enables significant reduction in the variability of key device metrics such as on-off current ratio and threshold voltage, as demonstrated in Figure 2.3 (c) and (d), respectively.

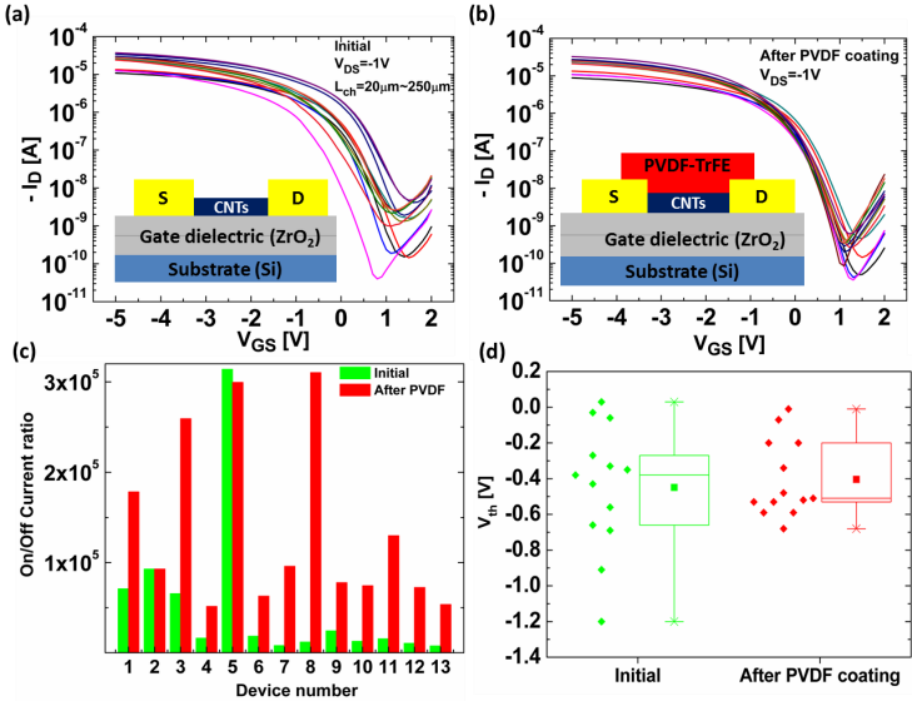

Figure 2.3: Electrical characteristics of SWCNT FETs with spin coated P(VDF-TrFE) on top of the active semiconductor layer. (a) and (b) are I_D-V_{GS} curves of SWCNT FETs before and after P(VDF-TrFE) spin-coating, respectively (Insets show the device structures). (c) On/Off current ratio before and after P(VDF-TrFE) spin-coating. (d) Effect of spin-coated P(VDF-TrFE) on threshold voltage (V_{th}) distributions of SWCNT FETs. The box chart indicates the average of V_{th} (solid square), minimum and maximum values (cross), and the range from 25% to 75% (box).

The spin-coated P(VDF-TrFE) films on SWCNT FETs not only reduce the threshold voltage by 10%, but also improve the threshold voltage variation by 45%. In addition, the on-off current ratio is enhanced along with a reduction in the off-current. These favorable changes are seen only after the annealing step, indicating that the annealing step is a critical processing step.

Similar improvements are also seen when the P(VDF-TrFE) capping layer is inkjet printed, as shown in Figure 2.4.

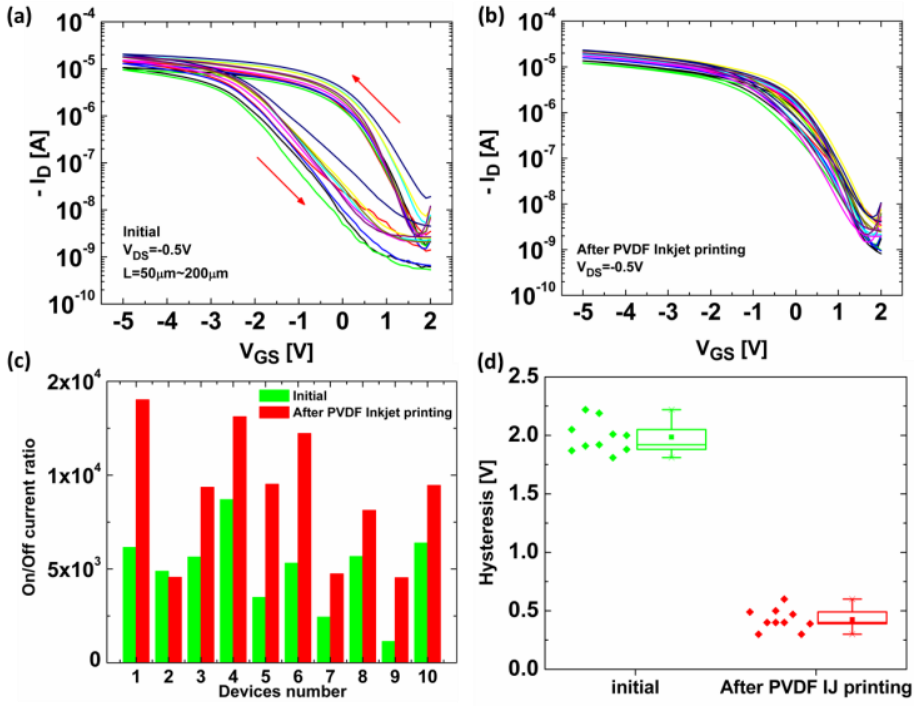

Figure 2.4: Electrical characteristics of SWCNT FETs with inkjet printed P(VDF-TrFE) on top of the semiconductor layer. (a) and (b) are double swept I_D-V_{GS} curves of SWCNT FETs before and after P(VDF-TrFE) inkjet printing, respectively. (c) On/Off current ratio before and after P(VDF-TrFE) inkjet printing. (d) Effect of inkjet printed P(VDF-TrFE) on the hysteresis of SWCNT FETs. The box chart indicates the average of V_{th} (solid square), minimum and maximum values (cross), and the range from 25% to 75% (box).

The reduction in variability of device characteristics and in the degree of hysteresis is even more pronounced in this case. Figure 2.4 (a) and (b) illustrate the changes in the transfer characteristics of the SWCNT FETs after P(VDF-TrFE) inkjet printing and annealing. The off-current is decreased and the threshold voltage variation is reduced without on-current degradation, similar to the effects produced by spin-coated P(VDF-TrFE). As shown in Figure 2.4 (d), hysteresis is reduced by 78% in the SWCNT FETs with an inkjet printed P(VDF-TrFE) capping layer

2.3.2. Gate bias stability

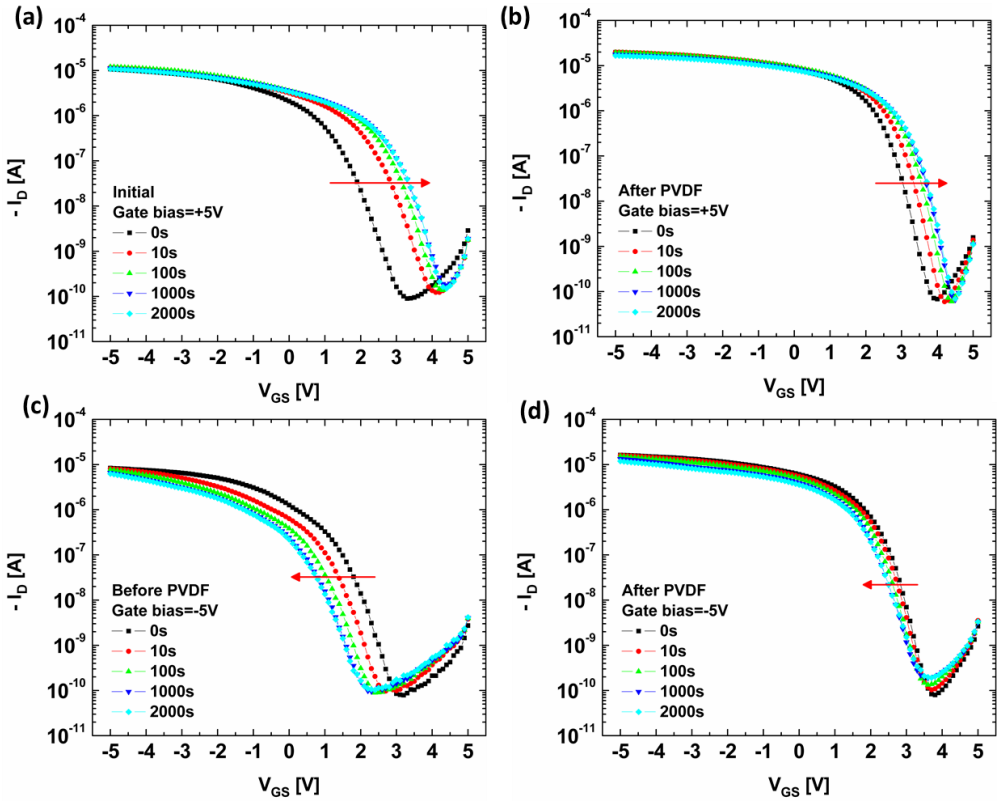

Figure 2.5: Transfer characteristics during the gate bias stress on SWCNT FETs with and without inkjet printed P(VDF-TrFE) cap layer. (a) and (b) are positive gate bias stress on SWCNT FETs with and without inkjet printed P(VDF-TrFE) cap layer, respectively. (c) and (d) are negative gate bias stress on SWCNT FETs with and without P(VDF-TrFE), respectively.

The passivation benefit of inkjet printed P(VDF-TrFE) capping layer is also studied in terms of gate bias stability of SWCNT FETs.

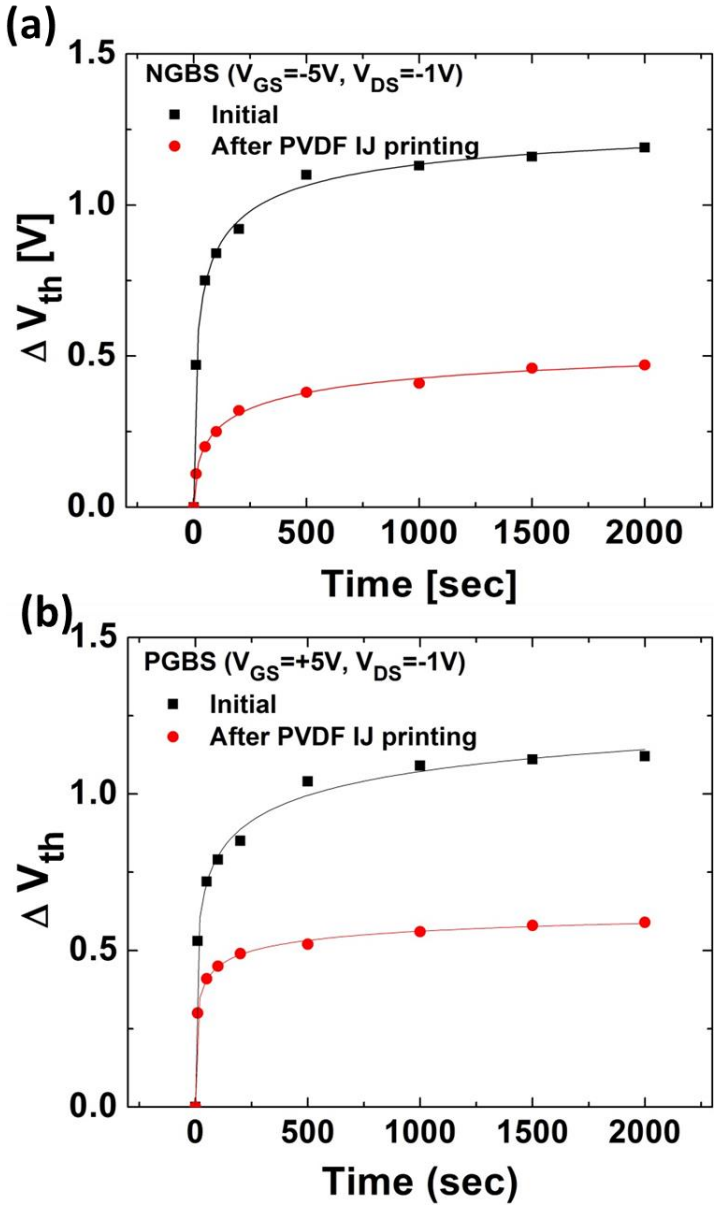

Figure 2.6: The passivation benefits of inkjet printed P(VDF-TrFE) on gate bias stress stability. Threshold voltage shift (ΔV_{th}) with stress time under (a) positive gate bias stress (PGBS) and (b) negative gate bias stress (NGBS). The magnitude of the gate bias was fixed at ± 5V (1.85 MV/cm), and V_{DS} was fixed at -1 V.

The shifts in threshold voltage (ΔV_{th}) under positive and negative gate bias are also substantially reduced, by 47% and 60%, respectively. These results are illustrated in Figure 2.5 and Figure 2.6. Hydrophobic surface characteristics of P(VDF-TrFE) can effectively prevent device from absorbing water / oxygen molecules in the air, resulting in the improvement on device stability as well as hysteresis.

2.3.3. Origin of improvements in fluoropolymer capping

We have also performed a series of experiments aimed at understanding the mechanisms underlying the observed improvements. Our initial hypothesis was that the polar nature of the fluoropolymer was responsible for the improvements discussed above. The dipolar nature of the fluoropolymer neutralizes charged impurities and defects, thereby resulting in a reduction in off-current and hysteresis. The annealing step provides sufficient energy for the polymer molecules to adopt energetically favorable orientations with respect to the SWCNTs that result in the observed modifications to device properties.

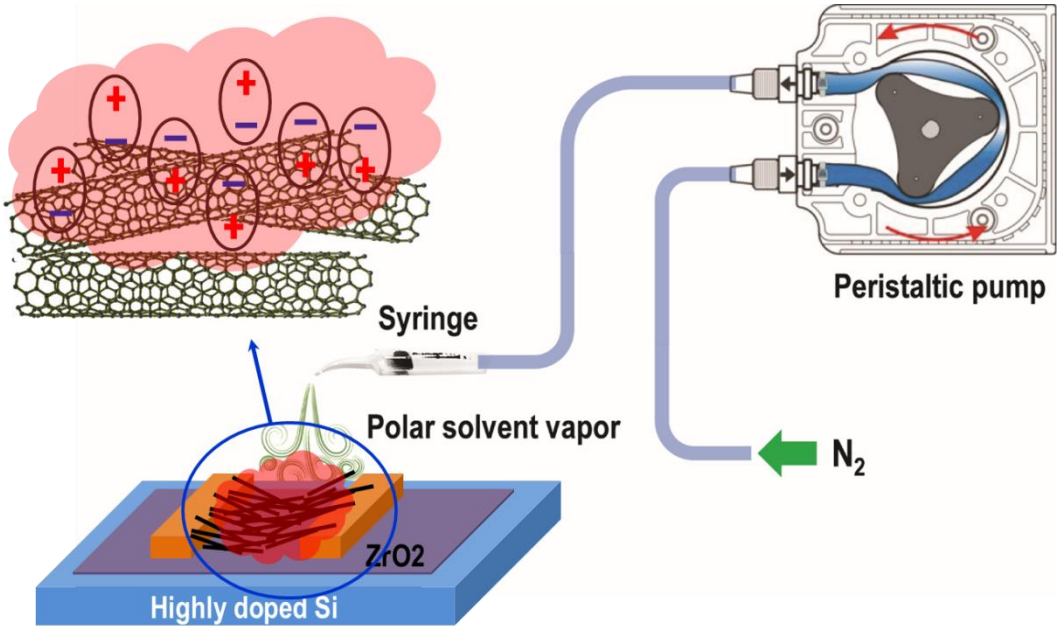

Figure 2.7: Experimental set-up for vapor exposure test of SWCNT FETs.

To test this hypothesis, we evaluated the device characteristics of the SWCNT FETs when exposed to various molecules with different dipole moments. These molecules were delivered as saturated vapors in nitrogen by means of a peristaltic pump as illustrated in Figure 2.7. The off-current is reduced dramatically (by up to a factor of 20) upon delivery of the most polar molecules (acetone and ethanol) while it remained unchanged for delivery of a non-polar molecule such as hexane. When the device is in the off-state, these dipolar molecules will partially neutralize charged dopants. The experimental data, shown in Figure 2.8, is consistent with this picture.

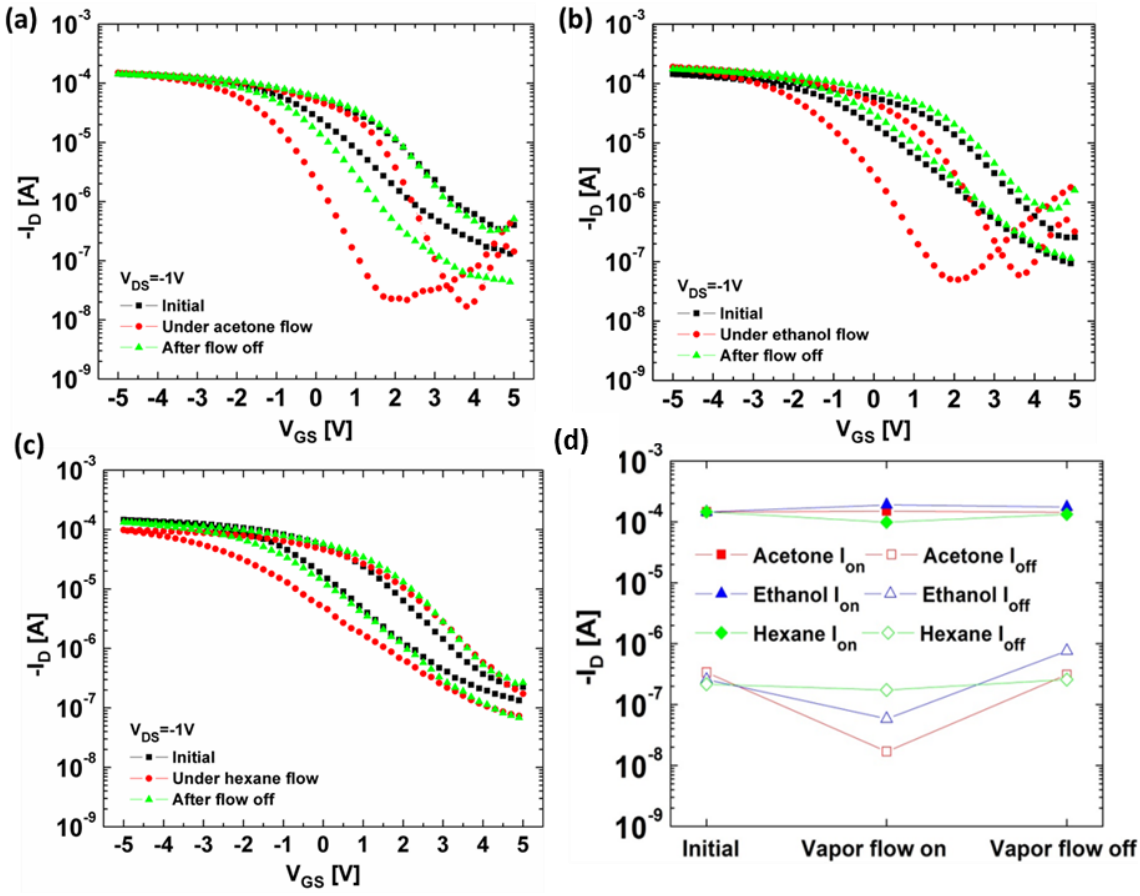

Figure 2.8: Vapor phase organic solvent exposure test on a SWCNT FET. Transfer characteristics were measured prior to, during, and after the vapor flow on the SWCNT FET; (a) acetone, (b) ethanol and (c) hexane. (d) On-state current (solid symbols) and off-state current (open symbols) extracted from transfer curves were compared.

The decrease in off-state current is proportional to the dipole moment of these molecules. Dipole moments (in units of Debye) of acetone, ethanol and hexane are 2.88, 1.69 and ≈0, respectively [52, 53]. Since these small molecules can reorient themselves when the electric field direction is switched, we would expect the hysteresis window to increase with the delivery of polar molecules in agreement with our experimental

observations as shown in Figure 2.9. In the case of annealed P(VDF-TrFE) capping layers, the molecular orientation of the P(VDF-TrFE) is unaltered since it is a capping layer and the electric fields across it are small. We hypothesize that the molecules adopt an orientation that partially neutralize charged impurities.

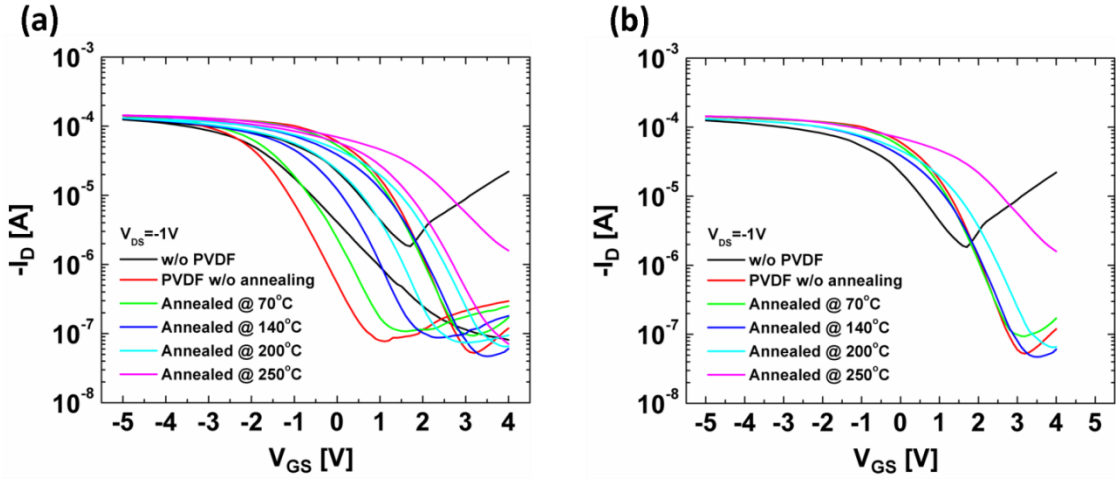

Figure 2.9: Transfer characteristics of the SWCNT FETs with various annealing temperatures of P(VDF-TrFE). (a) double-swept transfer curves starting from V_{GS}=4V showing the gate hysteresis. (b) single-swept transfer curves starting from V_{GS}=4V.

2.3.4. Circuit characteristics with fluoropolymer capping

A reduction in device-to device variability, the magnitude of hysteresis, bias stress effects and off-current level that accompanies the use of fluoropolymer capping layers should provide beneficial effects on circuit performance. Circuits require the operation of many transistors in unison and all the above changes will benefit the yield (percentage of circuits that operate properly) and the operating characteristics. 5-stage ring oscillators (ROSC) based on inkjet printed CNTs and amorphous zinc tin oxide (ZTO) complementary circuits were fabricated and characterized to investigate the effect of P(VDF-TrFE) top coating on circuit performance. Detailed information of the inkjet

printed ROSC was described in our previous work [54]. As shown in Figure 2.10, ring oscillators with a small oscillation amplitude before fluoropolymer deposition show a significant increase (from 0.31 V to 1.11 V on average) in oscillation amplitude. The oscillation frequency also increases by 42%, from 42 kHz to 60 kHz, due to improvements in the on and off state characteristics of the SWCNT FETs.

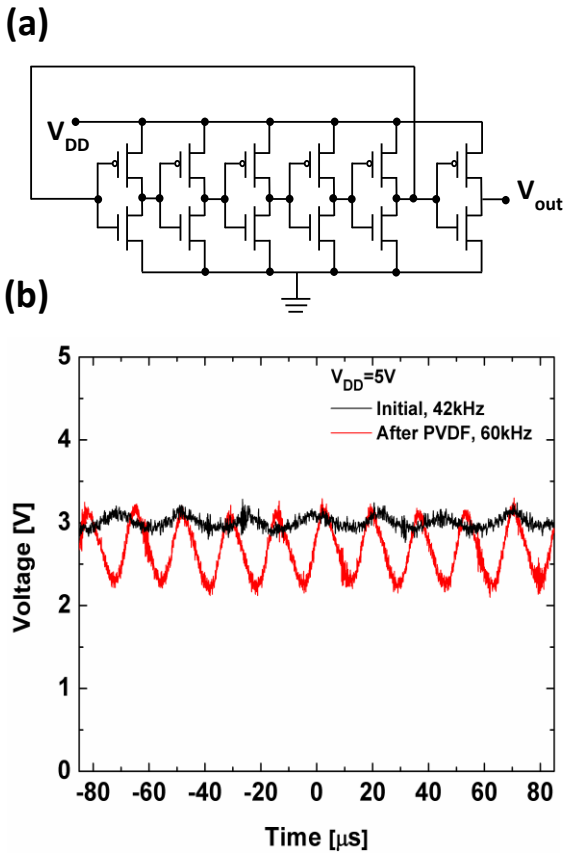

Figure 2.10: (a) Circuit diagram of a five-stage ring oscillator. (b) The output signal of a five-stage ring oscillator based on SWCNTs and ZTO complementary circuit with spin coated PVDF.

2.4. CONCLUSION

In conclusion, we have shown that the use of coatings of the fluoropolymer containing copolymer P(VDF-TrFE) results in substantial improvements in the characteristics of SWCNT FET devices and circuits comprised of these devices. At the device level, there is a significant decrease in the following: (a) Off-current magnitude; (b) Degree of hysteresis; (c) Variation in threshold voltage; and (d) Bias stress degradation. We attribute this to the effects of oriented polar C-F bonds in the P(VDF-TrFE) which partially neutralize charges impurities and defects in the semiconductor and the semiconductor-gate insulator interface. Experiments investigating the effects of polar vapors on device characteristics support this model. At the circuit level, the improved uniformity in device characteristics plus the effects listed above, result in improved performance of 5-stage complementary ring oscillator circuits. The oscillation frequency and amplitude of complementary ring oscillators with SWCNT components increased by 42% and 250%, respectively. The use of such capping layers will be greatly beneficial to the adoption of SWCNT based circuits for a variety of applications.

Chapter 3. Inkjet Printed Short Channel Carbon Nanotube Field Effect Transistors*

3.1. INTRODUCTION

The field of printed electronics has advanced greatly over the past decade. The charge carrier mobilities achievable with printable semiconducting materials are now on the order of 10 cm^2/V-s and circuit operating frequencies in the MHz range have been reported [54]. Some applications in printed electronics require higher speed operation, thus necessitating new approaches that enable short channel transistors based on printed semiconductors. Additionally, current solution processing methods (*e.g.* spin-coating and solution casting) consume large quantities of high-value semiconductor materials and/or are not compatible with roll-to-roll processing (*e.g.*, dielectrophoresis). In our work, the SWCNT materials utilization is about two orders of magnitude more efficient**.**

Some example applications in printed electronics that require high-speed performance include rectifiers, frequency dividers in radio-frequency tags (which operate at GHz frequencies), and local high frequency oscillators. In principle, such components can be efficiently realized through inkjet printing of semiconducting SWCNT active layers with short channel lengths where individual nanotubes span the channel. In this Letter, we report a technique that achieves this goal while consuming picogram quantities of SWCNTs by fabricating short channel FETs based on inkjet printed SWCNTs. In contrast with previous reports of SWCNT FETs with small channel lengths [7, 9, 19, 55],

* This chapter is based on Reference 44: Jang, S.; Kim, B.; Geier, M. L.; Hersam, M. C.; Dodabalapur, A. Short Channel Field-Effect-Transistors with Inkjet-Printed Semiconducting Carbon Nanotubes. *Small,* **2015**, *11*, 5505-5509. S.J. and A.D. designed the experiments. S.J. carried out fabrication and characterization of devices. B.K. helped with ink preparation. M.L.G. and M.C.H. provided semiconducting SWCNTs.

our approach is the first short channel investigation utilizing roll-to-roll compatible inkjet printing of the SWCNT active material.

In this chapter, the active semiconductor channel consists of several randomly oriented inkjet printed semiconducting SWCNTs extending between source and drain (S/D) electrodes without forming a network of SWCNTs. This geometry is in contrast to previously reported inkjet printed SWCNT FETs with larger channel lengths in which the channel consists of a random network of interconnected SWCNTs [24, 27, 43, 56]. These devices are the shortest channel length SWCNT FETs reported in which the active material is deposited by inkjet printing. We construct SWCNT FETs employing two different device structures to compare the fabrication process and device characteristics of top-gate/bottom-contact and bottom-gate/top-contact devices as shown in Figure 3.1. In these structures, electron beam lithography (EBL) has been used to define the source-drain gap; however, similar source/drain spacing can be realized by high throughput processes such as nanoimprint lithography [57, 58]. We also develop a strategy for droplet confinement to achieve exceptionally low levels of SWCNT ink consumption during the single-pass inkjet printing of the SWCNT FETs.

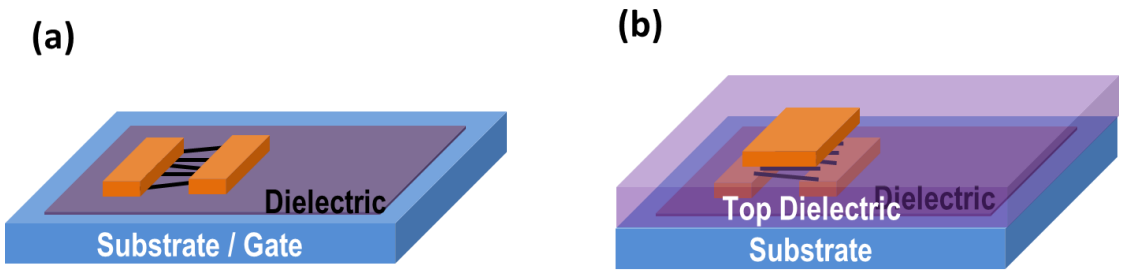

Figure 3.1: Device configurations for short channel SWCNT FETs. (a) Bottom-gate/top-contact. (b) Top-gate/bottom-contact

3.2. EXPERIMENTAL

3.2.1. Bottom-gate/top-contact structure

In order to fabricate the top contact devices by inkjet printing, SWCNT ink is printed on to a dielectric layer first and the exact locations of printed SWCNTs are confirmed using scanning electron microscopy to form S/D electrodes on the nanotubes. Figure 3.2 illustrates the schematic process flow for the fabrication of an inkjet printed SWCNT FET with bottom-gate/top-contact device structure. Heavily doped Si substrates were used as a global gate in the bottom-gate/top-contact device configuration. The gate dielectric consists of a double layer of high-κ ZrO_2 dielectric deposited from solution by a sol-gel route. The thickness and relative dielectric constant of the ZrO_2 were 90 nm and 18.2, respectively. The dielectric surface was then treated by UV O_3 in air for 10 minutes to modify its surface characteristics to achieve a spatially uniform distribution and modest concentration of SWCNTs after inkjet printing. In particular, a 10 pL drop of SWCNT ink (0.1 mg mL^{-1}, >98% purity semiconducting and achieved by density gradient ultracentrifugation) is printed onto the ZrO_2 substrate to form the channel layer.

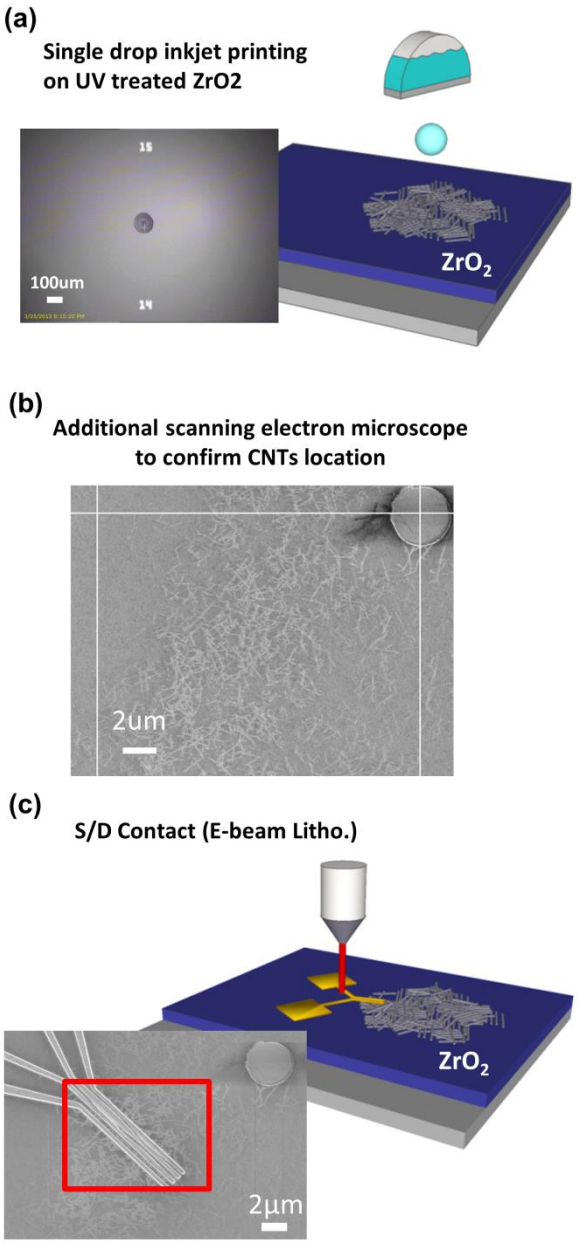

Figure 3.2: Schematic illustrations and images showing the process flow for inkjet printed SWCNT FET with bottom-gate/top-contact device structure. (a) Single drop inkjet printing of the SWCNT ink onto ZrO_2 dielectric. (Inset) Optical image of the inkjet printed droplet (10 pL). (b) SEM image to confirm the exact location of printed SWCNTs. (c) Electron beam lithography process to pattern S/D electrodes onto printed SWCNTs. (inset) SEM image showing the completed device (red square).

While the concentration of SWCNTs in the channel is readily controlled by the size of the rectangular perimeter in the top-gate/bottom-contact structure, surface treatment of the substrate and printing conditions are especially critical in the bottom-gate/top-contact structure. The size of the semiconducting film formed by inkjet printed single droplet can be effectively controlled by UV O_3 surface treatment and the temperature of the printing plate as shown in Figure 3.3 and Figure 3.4.

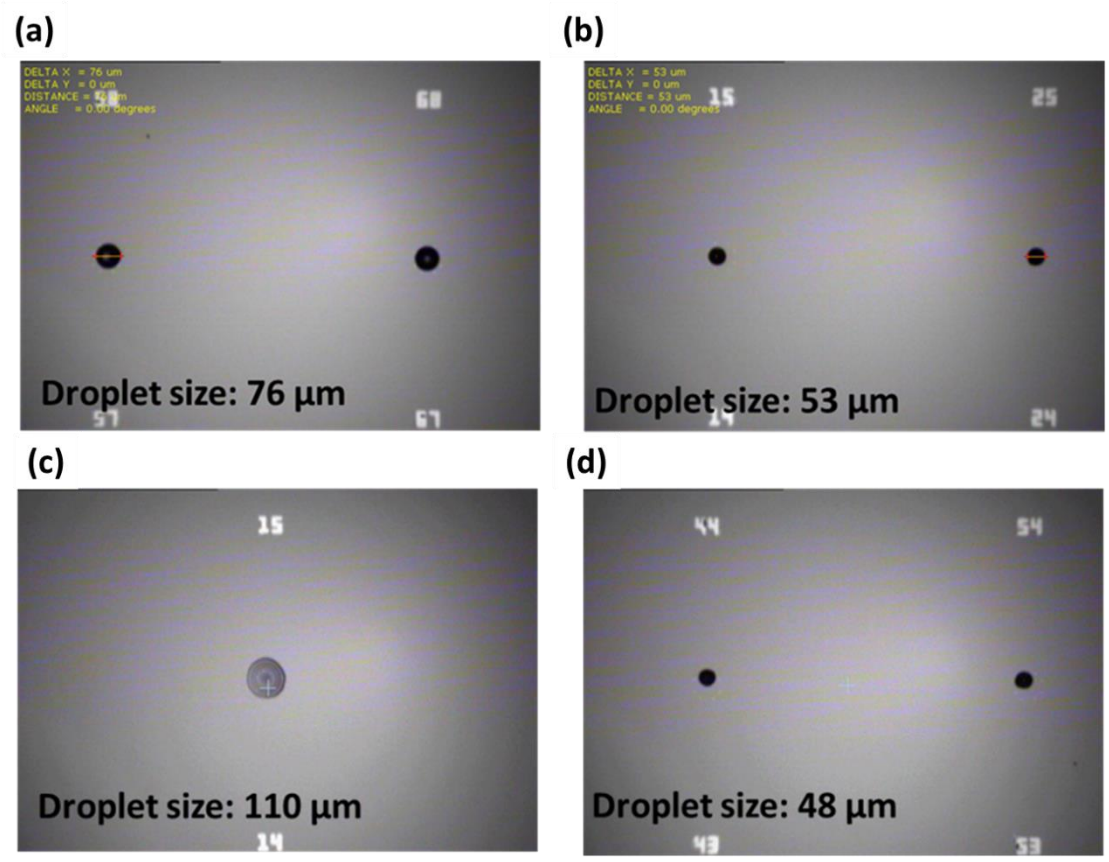

Figure 3.3: Optical images of 10 pL inkjet printed droplets of SWCNT ink (a) on UV O_3 treated substrate at 21^{o}C printing plate temperature, (b) on untreated substrate at 21^{o}C printing plate temperature, (c) on UV O_3 treated substrate at 60^{o}C printing plate temperature, (d) on untreated substrate at 60^{o}C printing plate temperature.

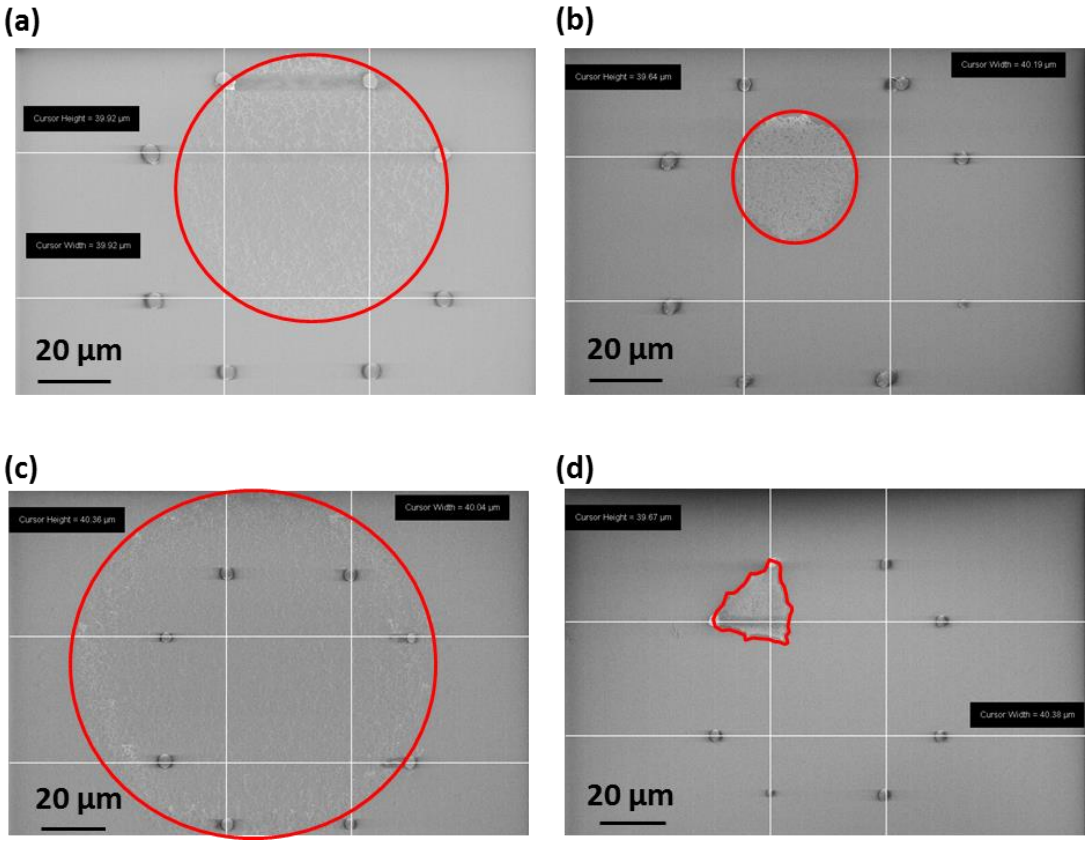

Figure 3.4: Scanning electron microscope (SEM) images of 10 pL inkjet printed droplets of SWCNT ink (0.1 mg mL^{-1}) (a) on UV O_3 treated substrate at 21°C printing plate temperature, (b) on untreated substrate at 21°C printing plate temperature, (c) on UV O_3 treated substrate at 60°C printing plate temperature, (d) on untreated substrate at 60°C printing plate temperature. Areas of SWCNTs are outlined with red lines.

Surface energy modification by the UV O_3 treatment was investigated by contact angle measurements. Using a contact angle goniometer (model FTA 200, First Ten Angstrom Inc.), contact angles of different liquids on untreated, UV O_3 treated, oxygen plasma treated ZrO_2 surfaces were measured (Figure 3.5(a)). To calculate the surface energy of each ZrO_2 surface, contact angles of two different liquids, deionized water and ethylene glycol, were measured. Surface energies of untreated, UV O_3 treated and oxygen

plasma treated ZrO_2 surfaces were calculated to be 48.3 mJ m^{-2}, 53.0 mJ m^{-2} and 75.9 mJ m-2, respectively. The surface energy values are calculated from contact angle analysis using two liquids method based on the Young's equation and Fowke's theory[59, 60] as following equation (eq. 3.1):

$$\gamma_1(1+\cos\theta) = 2\left\{\sqrt{\gamma_L^d \gamma_S^d} + \sqrt{\gamma_L^P \gamma_S^P}\right\} \qquad \text{(eq. 3.1)}$$

As shown in Figure 3.5 (b), UV O_3 treatment might be the most effective method to increase the surface energy of the ZrO_2 substrate.

This increase in surface energy contributes to the control of the droplet size on the ZrO_2 surface and enhances droplet pinning resulting in uniform distribution of SWCNTs in the dried droplet. The printing substrate is heated up to 60 °C to achieve an optimal final concentration of dried SWCNTs.

(a)

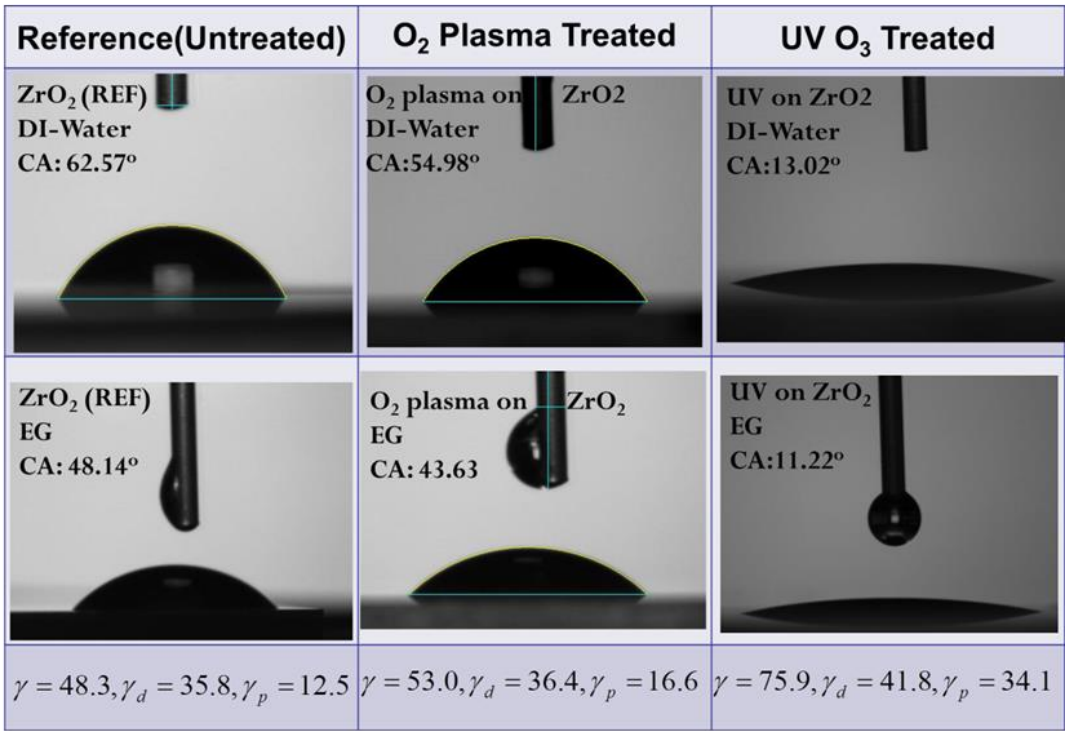

(b)

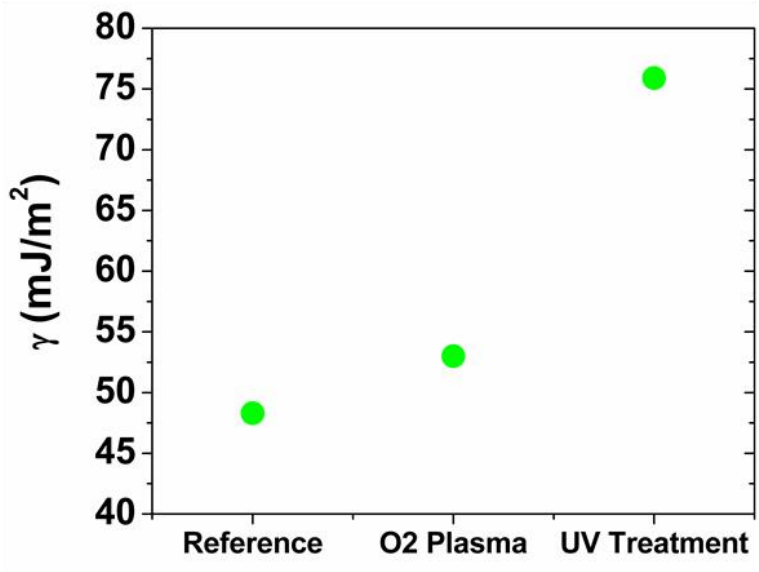

Figure 3.5: Surface energy analysis of ZrO_2 substrates. (a) Contact angle measurement of various ZrO_2 substrates using deionized water and ethylene glycol. (b) Calculated surface energy based on contact angle measurements.

After deposition of SWCNTs, scanning electron microscopy was performed to confirm the exact location as shown in Figure 3.2 (b). Based on the spatial location of SWCNTs extracted from the scanning electron microscope images, source and drain (S/D) contacts consisting of Ti/Pd (10 nm/50 nm) was patterned by EBL and lift-off (Figure 3.2 (c)).

3.2.2. Top-gate/bottom-contact structure

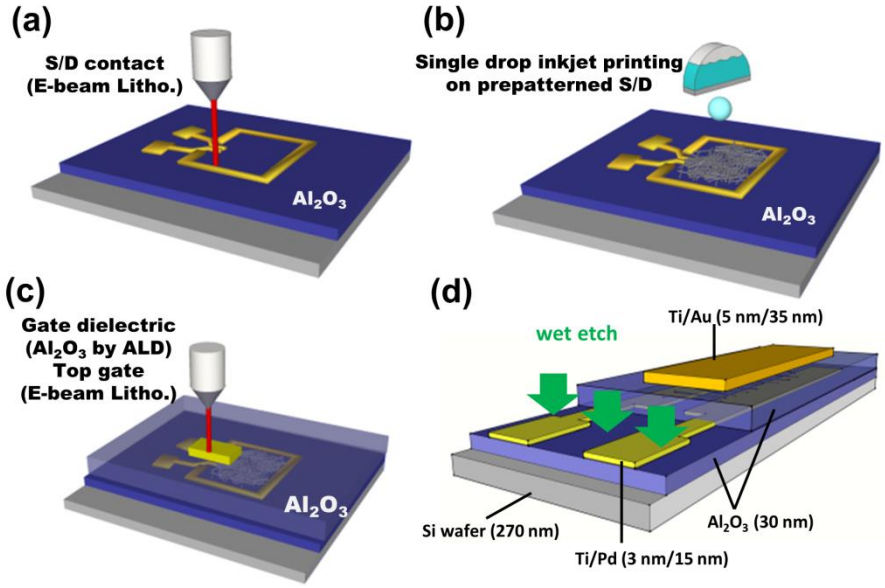

Figure 3.6: A schematic illustration of the process flow for inkjet printed a SWCNT FET with top-gate/bottom-contact device structure. (a) Electron beam lithography (EBL) is used to pattern S/D electrodes on the Al_2O_3 substrate. (b) Single drop (10 pL) inkjet printing of SWCNTs on the prepatterned S/D area. (c) Deposition of top dielectric, 30 nm thick Al_2O_3, by ALD and top gate electrode patterned by EBL. (d) Wet etching process with hydrofluoric acid to form via holes for probe contact pads.

A schematic process flow to fabricate inkjet printed SWCNT FETs with a top-gate/bottom-contact configuration is illustrated in Figure 3.6. Heavily doped Si substrates covered by 30 nm thick Al_2O_3, deposited by atomic layer deposition (ALD), were used as the substrate in the top-gate/bottom-contact configuration. S/D electrodes consisting of Ti/Pd (3 nm/15 nm) were patterned by EBL and lift-off on the Al_2O_3 substrate prior to inkjet printing of the SWCNTs. As shown in Figure 3.6 (a), a rectangular shaped metal line feature (60 μm × 60 μm) was patterned along with S/D electrodes in the same lithography step. The purpose of this additional structure is to confine the inkjet printed droplet to the S/D area. After the deposition of S/D electrodes, the substrate was UV O_3 treated to modify the surface energy of the Al_2O_3. Highly enriched semiconducting SWCNTs (>98% purity, achieved by density gradient ultracentrifugation [21, 22]) dispersed in 1-cyclohexyl-2-pyrrolidone (CHP) were inkjet printed onto the prepatterned S/D area using a FUJIFILM Dimatix Material Printer (DMP-2831) in air. As illustrated in Figure 3.6 (b), one 10 pL drop of SWCNT ink (0.05 mg mL^{-1}) is printed to form the channel layer. The top dielectric, Al_2O_3, was deposited on the inkjet printed SWCNTs by ALD(Savannah^{TM}, Cambridge Nano Tech Inc.) using trimethylaluminum (TMA) as a precursor. ALD was performed at a temperature of 200 °C with pulse of H_2O for 15 ms and TMA for 25ms. The thickness and relative dielectric constant of the Al_2O_3 were 30 nm and 7.8, respectively. The top gate electrode, a bilayer of Ti/Au (5 nm/35 nm), was patterned by EBL and lift-off followed by a wet etching step with hydrofluoric acid to form via holes for probe contact pads as shown in Figure 3.6 (c) and (d).

3.2.3. Electron beam lithography

Global alignment marks for electron-beam lithography consisting of a Cr/Pt (5 nm/35 nm) double layer were patterned by conventional photolithography and lift-off process. Source and Drain (S/D) regions with a channel length of 150-250 nm were patterned into poly(methyl methacrylate) (950PMMA A6, Microchem Crop.) using electron beam lithography (EBL, Raith Nanofabrication). Electron-beam evaporation was then used to sequentially deposit titanium and palladium, followed by lift-off in acetone at 60 °C.

3.3. RESULTS AND DISCUSSION

3.3.1. Material consumption of solution processing methods.

Comparison of SWCNT material consumption for common solution-processing methods is shown in Table 3.1. In order to fabricate a single device on a 8 mm × 8mm substrate, 10 pL of solution containing 0.5 pg of SWCNTs is required for inkjet printing in this work, while spin-coating and solution casting consume 6 µL of solution containing 0.3 µg of SWCNTs and 10 µL of solution containing 0.5 µg of SWCNT, respectively. To further facilitate this comparison, the material consumption normalized by area for inkjet printing, spin-coating and solution casting are approximately 0.14 ng mm^{-2}, 4.69 ng mm^{-2} and 7.81 ng mm^{-2}, respectively. Therefore, inkjet printing shows a ~2 orders of magnitude improvement in material utilization.

Table 3.1: Required volume of solution and estimated weight of SWCNTs for common solution-processing methods.

Methods	Volume of solution	Weight of SWCNTs	Covered area	Normalized Volume (µL mm^{-2})	Normalized Weight (µg mm^{-2})
Inkjet printing	10 pL	0.5 pg	60 µm x 60 µm	2.78E-03	1.39E-04
Spin-coating	6 µL	0.3 µg	Before spin: 5 mm x 5 mm (After spin: 8 mm x 8mm)	Before spin: 2.40E-01 (After spin: 9.38E-02)	1.20E-02 → × 86.4* (4.69E-03 → × 33.8*)
Solution casting	10 µL	0.5 µg	8 mm x 8 mm	1.56E-01	7.81E-03 → × 56.3*

*Red numbers represent the multiplying factors of material consumption compared to Inkjet printing.

3.3.2. Bottom-gate/top-contact structure

The channel length between the S/D electrodes patterned on the inkjet printed SWCNTs were 250 nm. The electrical characteristics of inkjet printed SWCNT FETs with bottom-gate/top-contact device structure are shown in Figure 3.7.

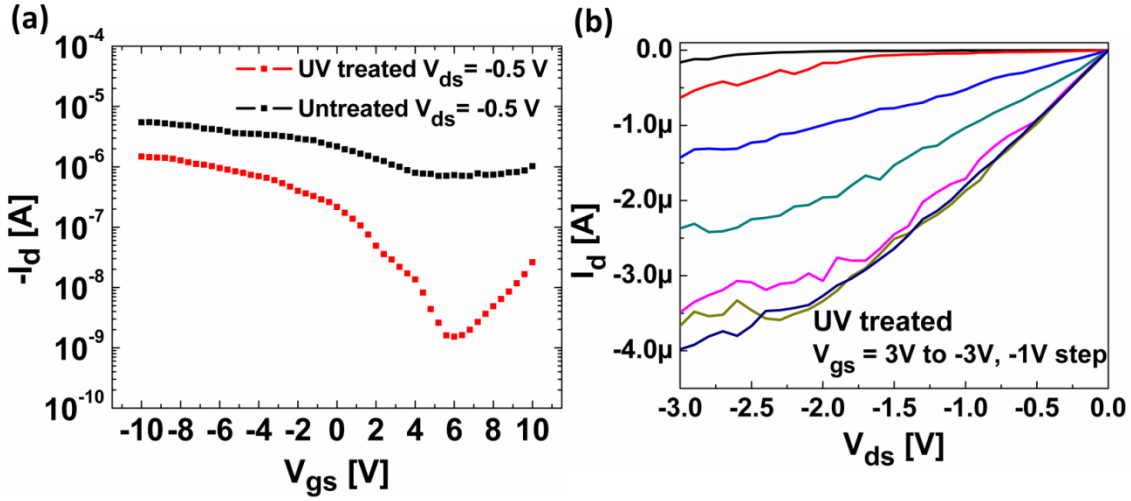

Figure 3.7: Electrical characteristics of inkjet printed SWCNT FETs with bottom-gate/top-contact device structure (L_{ch} = 250 nm). (a) Measured I_d-V_g transfer characteristics of UV O_3 treated (red squares) and untreated (black squares) SWCNT FETs. (b) Measured I_d-V_d output characteristics of UV O_3 treated SWCNT FETs.

The transfer characteristics of devices fabricated on the UV O_3 treated and untreated ZrO_2 are compared in Figure 3.7 (a). The gate modulation of the channel current in the untreated device is weak, with I_{on}/I_{off} of less than 10, while the UV O_3 treated devices exhibit a stronger gate modulation of the channel current, with I_{on}/I_{off} of 10^3. This gate-voltage-independent channel current in the untreated device may be due to tube-to-tube screening caused by the high concentration of SWCNTs in the dried droplet resulting from the evaporation of solvent without adequate droplet pinning (Figure 3.8).

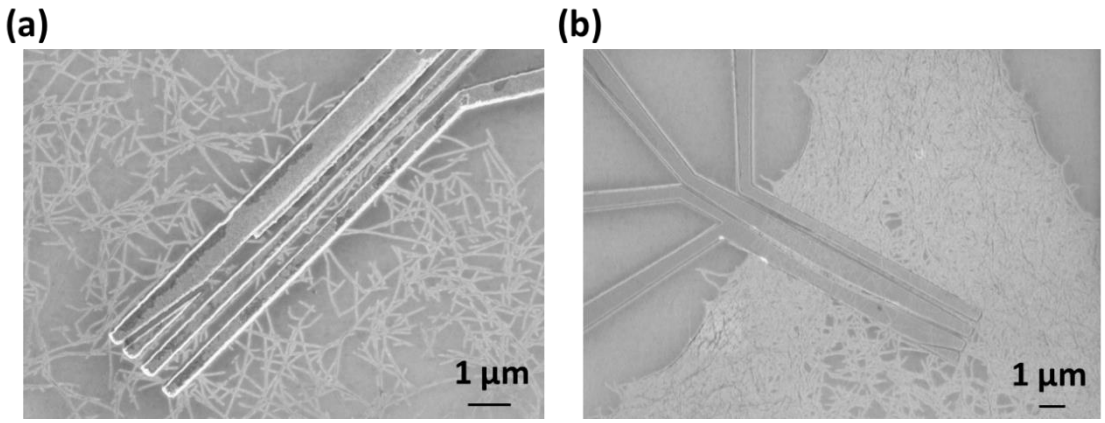

Figure 3.8: SEM images showing the difference in concentration of SWCNTs according to UV O_3 treatment: (a) with UV O_3 treatment, (b) without UV O_3 treatment.

Although these devices have short channel lengths with individual SWCNTs spanning the entire channel, the impact of UV O_3 treatment is quite similar to that in longer channel length devices which have random network SWCNTs in the channel [27]. For the UV O_3 treated devices, the channel contains approximately 30 individual SWCNTs as counted by scanning electron microscopy in Figure 3.9, and have a linear field-effect mobility of 24 cm^2 / V-s at V_{ds} = -0.5 V.

The linear mobility value in these devices were extracted from the characteristics shown in Figure 3.7 (a) by the following equation (eq. 3.2):

$$\mu = \frac{L}{W} \times \frac{1}{C_{ox}} \times \frac{1}{V_D} \times \frac{dI_D}{dV_G} \qquad \text{(eq. 3.2)}$$

where μ is the linear field effect mobility, C_{ox} is the capacitance per unit area of gate dielectric, V_D is the drain voltage, I_D is the drain current and V_G is the gate voltage.

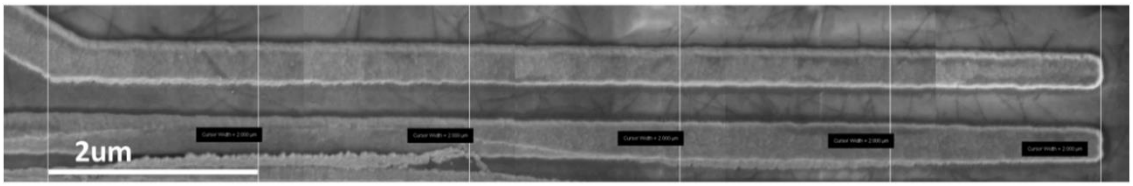

Figure 3.9: SEM image of the bottom-gate/top-contact device. Approximately 30 individual SWCNTs connect the S/D electrodes (L_{ch} = 250 nm).

3.3.3. Top-gate/bottom-contact structure

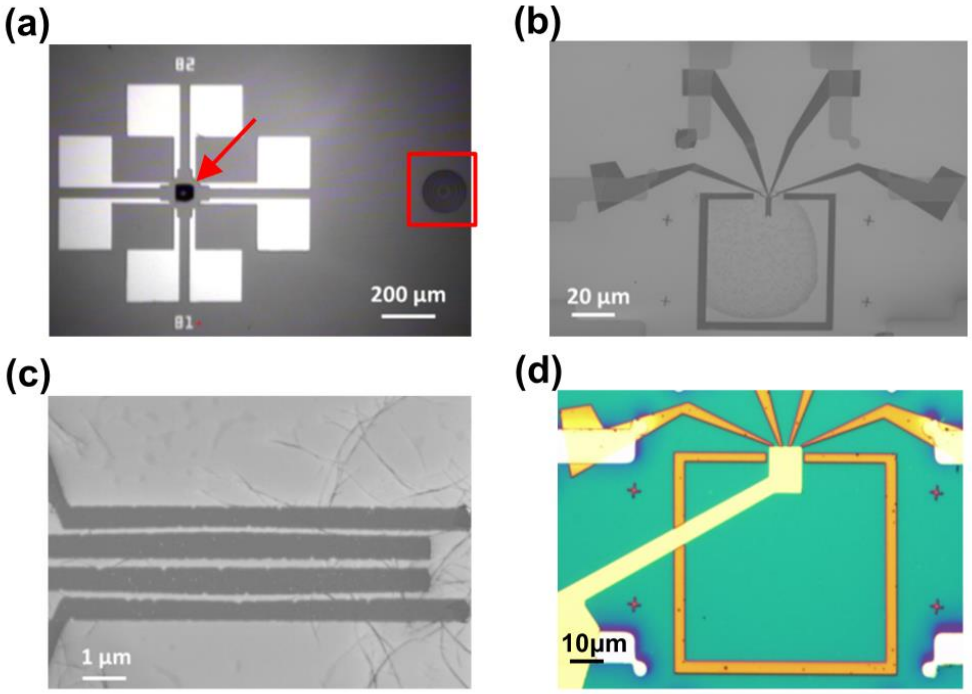

Figure 3.10: (a) Optical image of the inkjet printed droplets demonstrating droplet confinement by the prepatterned rectangular metal line structure. The diameter of the droplet without confinement on Al_2O_3 is 160 µm (red square), and is larger than the confinement area of 60 µm × 60 µm (red arrow). (b) Scanning electron microscope (SEM) image of an inkjet printed droplet confined within the rectangular area within which the S/D electrodes were prepatterned. (c) SEM image of SWCNTs extending between S/D electrodes. (d) Optical image of inkjet printed SWCNT FETs with top-gate/bottom-contact device structure.

Figure 3.10 (a) and (b) show the inkjet printed single droplet was effectively confined by the rectangular perimeter. This feature is essential to fabrication because without this perimeter to confine the droplet, the ink spreads and the resultant device performance is significantly degraded. This confinement is due to the surface energy difference between UV O_3 treated Al_2O_3 and Pd (which is less hydrophilic). The resulting FETs have a channel length of 150 nm - 190 nm, where an average of 10 individual SWCNTs span the S/D electrodes, as shown in Figure 3.10 (c). The geometric channel width of S/D electrodes is 8 μm: however, the effective channel width of the device can be considered as a sum of the diameters of SWCNTs in the channel.

The electrical characteristics of inkjet printed SWCNT FETs with a top-gate/bottom-contact device structure are shown in Figure 3.11. A SWCNT FET with channel length of 190 nm shows I_{on}/I_{off} of ~10^3 in Figure 3.11 (a) (3.7×10^3 at V_{ds} = -0.5 V and 1.3×10^3 at V_{ds} = -1 V). Transconductance (g_m) values that are normalized by the sum of diameter of SWCNTs (1.4 nm per SWCNT) exceed 150 μS μm^{-1} at V_{ds} = -1V with 10 SWCNTs as the active channel material.

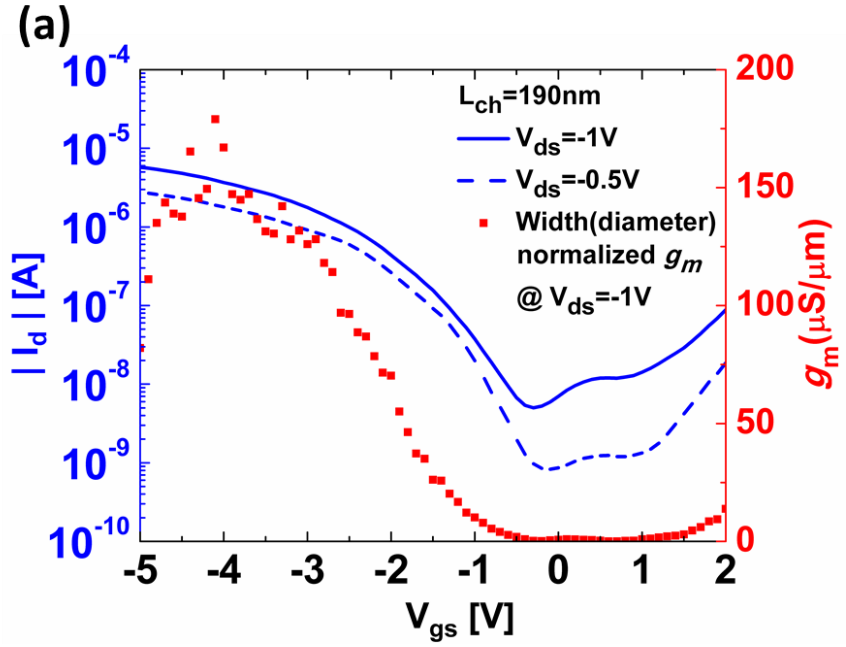
(a)
10^{-4}
10^{-5}
10^{-6}
10^{-7}
10^{-8}
10^{-9}
10^{-10}
| I_d | [A]
200
150
100
50
0
g_m(μS/μm)
L_{ch}=190nm
V_{ds}=-1V
V_{ds}=-0.5V
Width(diameter) normalized g_m @ V_{ds}=-1V
-5 -4 -3 -2 -1 0 1 2
V_{gs} [V]

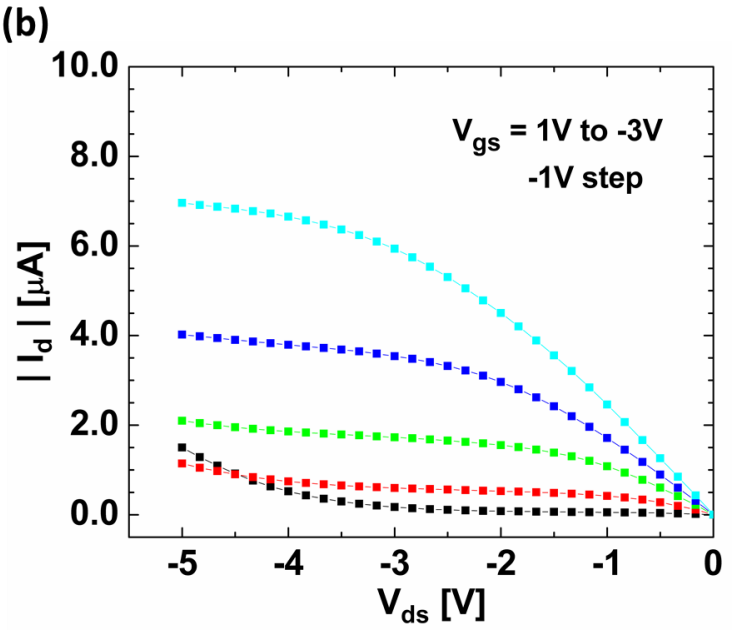
(b)
10.0
8.0
6.0
4.0
2.0
0.0
| I_d | [μA]
V_{gs} = 1V to -3V
-1V step
-5 -4 -3 -2 -1 0
V_{ds} [V]

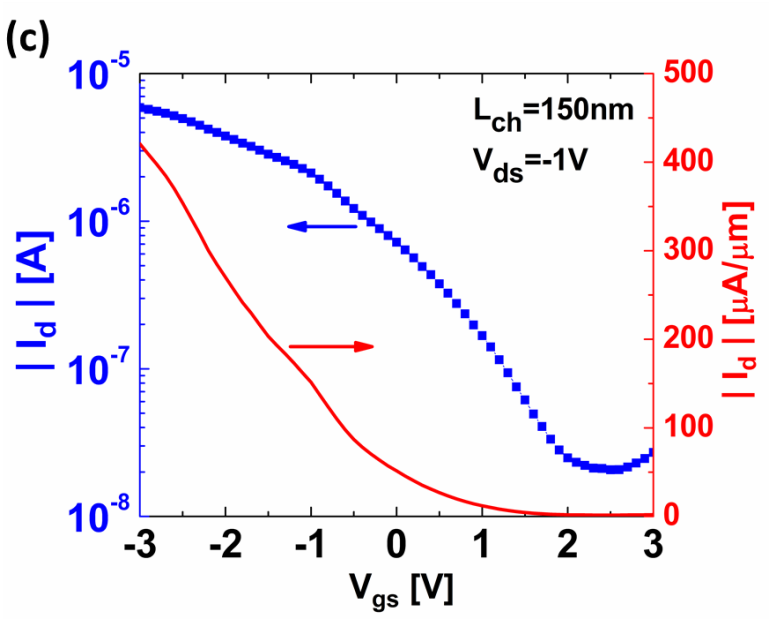

Figure 3.11: Electrical characteristics of inkjet printed SWCNT FETs with top-gate/bottom-contact device structure. (a) Measured I_d-V_g transfer characteristics (blue lines) and normalized transconductance g_m (red squares) for a 190 nm device. (b) Measured I_d-V_d output characteristics of a 190 nm device. (c) Measured I_d-V_g transfer characteristics (blue squares) and diameter-normalized current (red line) of a 150 nm device.

Figure 3.11 (b) shows output characteristics of SWCNT FET with a channel length of 190 nm and Figure 3.11 (c) shows the characteristics of a 150 nm channel length SWCNT FET. It may be noted that the 150 nm channel length device has a higher I_{on} at same V_{ds}; however I_{off} is also increased compared to the SWCNT FET with L = 190 nm. This trend is consistent with other results for SWCNT FETs based on individual SWCNTs [55]. Because inkjet printing deposits SWCNTs with a random orientation, SWCNTs may not be perpendicular to S/D electrodes and the actual value of channel length will be increased. Assuming the channel length is 190 nm, the linear field-effect mobility of this device is 209 cm^2 / V-s at V_{ds} = -0.5 V. This calculated mobility is

based on the assumption that the channel width is the sum of the diameters of all the SWCNTs (14 nm) that span the S/D gap.

Consequently, in terms of both performance characteristics as well as fabrication complexity, the top-gate/bottom-contact structure is superior to the bottom-gate/top-contact for inkjet printed short channel SWCNT FETs. In the bottom-gate/top-contact structure, SWCNTs can be damaged by electron irradiation during the EBL process to form S/D electrodes on SWCNTs [61, 62]. In contrast with the bottom-gate/top-contact structure, SWCNTs are deposited after EBL process for S/D electrode in the top-gate/bottom-contact structure. Moreover, since nanoimprint lithography can be used to prefabricate similar S/D feature sizes as those demonstrated in the top-gate/bottom-contact structure, the fabrication process in which SWCNTs are inkjet printed on prefabricated S/D electrodes in the top-gate/bottom-contact structure is more compatible with roll-to-roll processing than the conventional bottom-gate/top-contact structure.

3.4. CONCLUSION

In summary, we have demonstrated a method of inkjet printing submicron-scale SWCNT FETs with channel lengths of 150 nm - 250 nm, far less than the average length of SWCNTs (1.36 μm). In addition, the transistor electrode design implies minimal consumption of SWCNT ink (a single droplet of 10 pL ink containing 0.5 pg of SWCNTs), thus realizing one of the primary benefits of additive manufacturing.

The transconductance and mobility values of these short channel devices greatly exceed those of previously reported inkjet printed SWCNT FETs (Table 3.2), with the added benefit of roll-to-roll compatibility.

Table 3.2: Comparison on the performance of inkjet / aeosol-jet printed SWCNT FETs

Reference	Device structure	Channel length	Gate dielectric	Linear mobility	Printing method
[27] (Our previous work)	Bottom-gate/ bottom-contact	150 um	ZrO_2	23.6 $cm^2V^{-1}s^{-1}$ (Intrinsic)	Inkjet printing
[54] (Our previous work)	Bottom-gate/ top-contact	20 um	ZrO_2	1.7 $cm^2V^{-1}s^{-1}$ (Geometric)	Inkjet priting
[16]	Top-gate/ bottom-contact	10 um	Ion gel	20 $cm^2V^{-1}s^{-1}$ (Geometric)	Aerosol jet printing
[63]	Bottom-gate/ top-contact	60-120 um	HfO_2	46 $cm^2V^{-1}s^{-1}$ (Geometric)	Spray printing
[64]	Bottom-gate/ bottom-contact	160 um	HfO_2	43 $cm^2V^{-1}s^{-1}$ (Intrinsic)	Inkjet printing
[65]	Bottom-gate/ bottom-contact	500 um	SiO_2	4.2 $cm^2V^{-1}s^{-1}$ (Intrinsic)	Inkjet printing
This work	Top-gate/ Bottom-contact	150 nm~ 250 nm	Al_2O_3	~200 $cm^2V^{-1}s^{-1}$ (Geometric/Tube diameters)	Inkjet printing

We compared the fabrication process and characteristics of SWCNT FETs employing two different device structures, bottom-gate/top-contact and top-gate/bottom-contact, and found the top-gate/bottom-contact device to possess distinct advantages from both processing and performance perspectives. Overall, this work will impact ongoing efforts to realize high-performance electronic devices in a manner compatible with roll-to-roll additive manufacturing methods.

Chapter 4. Short Channel Ambipolar Transistors with Inkjet Printed Semiconducting Carbon Nanotubes*

4.1. INTRODUCTION

Single walled carbon nanotubes (SWCNTs) are promising materials for use in thin-film electronics applications [10, 23, 66-68]. They can possess relatively high carrier mobility and on/off current ratios [69-71]. In recent work, we showed that inkjet printed short channel length SWCNT FETs, in which the average nanotube length (~1.4 microns) is greater than the source/drain (S/D) spacing, exhibit high carrier mobilities in excess of 100 cm^2/V-s for holes [44]. The SWCNTs were deposited by inkjet printing, which is a very convenient and cost-effective method for fabricating FETs and circuits. Such devices are very promising to achieve high speed switching in printed electronics, which has hitherto been a limitation.

In this chapter, we firstly describe the fabrication and characteristics of high-performance ambipolar transistors with inkjet printed SWCNT active layers in top-gate/bottom-contact device configuration. To make the devices, SWCNTs were inkjet printed onto recessed S/D electrodes to achieve nominally flat SWCNTs in the channel and the Al_2O_3 top gate insulator was deposited by atomic layer deposition (ALD). These devices have channel lengths in the range 150-200 nm, well below the average nanotube length. We then describe and discuss the effects of nanotube distortion on the electrical properties of these SWCNT FETs.

---

* This chapter is based on Reference 45: Jang, S.; Kim, S.; Geier, M. L.; Hersam, M. C.; Dodabalapur, A. Inkjet Printed Carbon Nanotubes in Short Channel Field Effect Transistors: Influence of Nanotube Distortion and Gate Insulator Interface Modification. *Flex. Print. Electron. (Under review).* S.J. and A.D. designed the experiments. S.J. carried out fabrication and characterization of devices. S.K. helped with inkjet printing. M.L.G., and M.C.H. provided semiconducting SWCNTs.

We also study the effects of incorporating a thin fluoropolymer layer, poly(vinylidene fluoride-trifluoroethylene) (P(VDF-TrFE)), at the interface between the Al_2O_3 and the SWCNT.

We demonstrate that bent nanotubes possess degraded electron transport, in accordance with recent reports [61, 72]. Like distortion, incorporation of P(VDF-TrFE) has a similar effect in transforming ambipolar devices into dominantly p-channel type, although the mechanism is different.

4.2. EXPERIMENTAL

4.2.1. Device fabrication

Heavily doped Si substrates with thermally grown SiO_2 (270 nm thickness) were cleaned by sonication with acetone, 2-propaonl, and DI water. Global alignment marks for electron-beam lithography (EBL, Raith Nanofabrication) consisting of a Cr/Pt (5 nm/35 nm) double layer were patterned by conventional photolithography and lift-off process. Source and Drain (S/D) regions with a channel length of 150-200 nm were patterned into poly(methyl methacrylate) (950PMMA A4, Microchem Corp.) using EBL. Trench patterns for the recessed S/D electrodes were dry etched by CHF_3 plasma at 100 W for 30 sec. Electron-beam evaporation was then used to sequentially deposit titanium and palladium, followed by lift-off in acetone at 60 °C. SWCNTs (with >98% semiconducting SWCNTs sorted by density gradient ultracentrifugation) [21, 22] dispersed in 1-cyclohexyl-2-pyrrolidone (CHP) were deposited onto the recessed S/D electrodes using Fujifilm Dimatix DMP-2831 in air. 30 nm thick Al_2O_3 layer was deposited by atomic layer deposition (ALD, Savannah^{TM}, Cambridge Nano Tech Inc.) using trimethylaluminum (TMA) as a precursor. ALD was performed at a temperature of 200 °C with pulse of H_2O for 15 ms and TMA for 25ms. Top gate electrodes consisting Ti/Au (5 nm/35 nm) were patterned by EBL and lift-off processes. In order to form via holes for probe contact pads, Al_2O_3 top dielectric was etched with hydrofluoric acid. In particular, the sample was dipped into 1.25% aqueous hydrofluoric acid for 45 sec. to etch the 30nm thick Al_2O_3 layer.

4.2.2. Electrical characterization of devices

The electrical characteristics of SWCNT FETs were measured using a HP4155C semiconductor parameter analyzer. Measurements were performed under ambient conditions and in a vacuum environment (1×10^{-3} Torr).

4.3. RESULTS AND DISCUSSION

4.3.1. Conventional short channel SWCNT FETs

An illustrative fabrication process and electrical characteristics of conventional inkjet printed short channel SWCNT FETs with top-gate/bottom-contact structure are shown in Figure 4.1.

As shown in Figure 4.1 (a), a single drop of semiconducting SWCNT ink (with >98% semiconducting SWCNTs sorted by density gradient ultracentrifugation [21, 22]) ink (10 pL) was printed onto the prepatterned S/D area followed by top gate dielectric and top-gate electrode processes. The bottom-contact structure is advantageous to inkjet printing and also avoids potential SWCNT damage during the electron beam lithography (EBL) process. As shown in Figure 4.1 (b) and (c), the bottom-contact device primarily exhibits p-type dominant characteristics with top-gate operation. The black square symbols in Figure 4.1 (b) show the transfer characteristics measured using bottom Si substrate as a global gate before depositing top dielectric and top gate electrode. The poor gate modulation and drain current may be caused by suspension or bending of SWCNTs between S/D electrodes in the channel. In Figure 4.1 (d), scanning electron microscope (SEM) image of SWCNTs printed on the prepatterned S/D electrodes shows the bending of SWCNTs due to the surface relief of the S/D electrodes. Such bending could shift the

Fermi level of SWCNTs toward valance band [72], resulting in weak ambipolar but with p-type dominant characteristics as shown in Figure 4.1 (c).

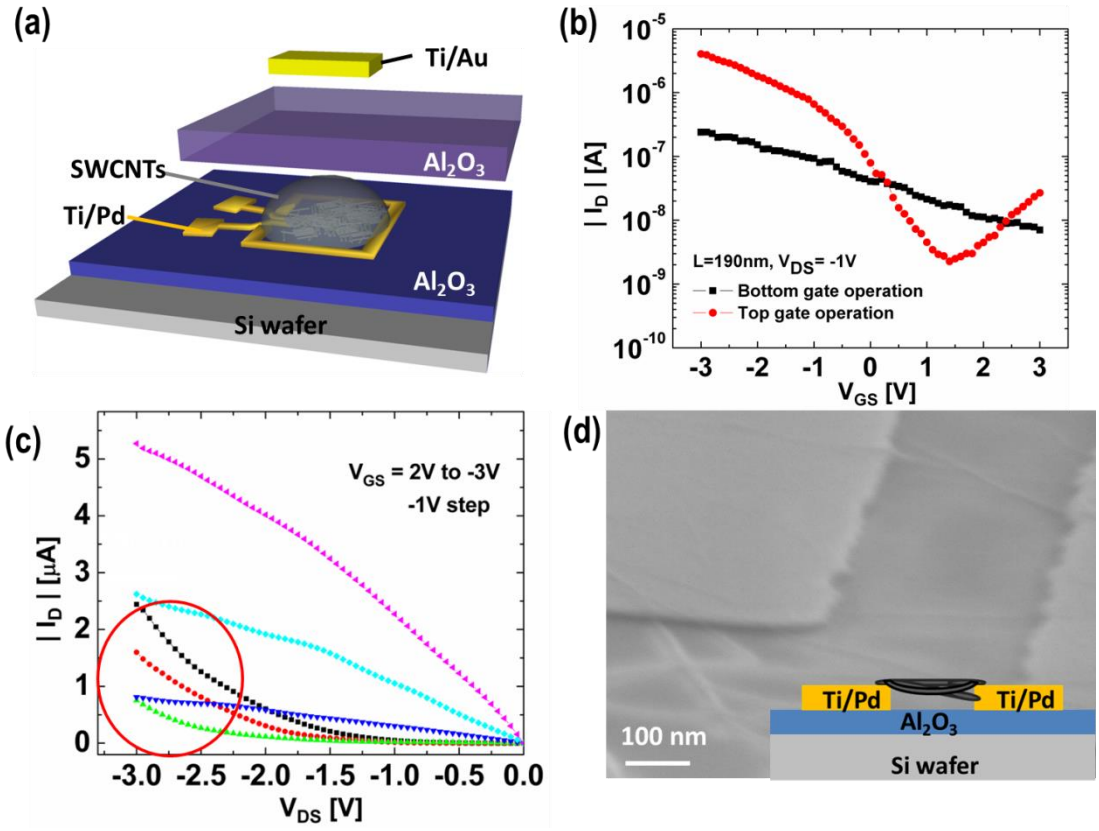

Figure 4.1: (a) Schematic illustration of the process flow for inkjet printed SWCNT FETs with top-gate/bottom-contact device structure. (b) Measured I_D-V_{GS} transfer characteristics of 190 nm channel length device showing the difference between bottom-gate operation (black squares) and top-gate operation (red circles). (c) Measured I_D-V_{DS} output characteristics of the 190 nm channel length device. The red circle indicates weak ambipolar characteristics. (d) SEM image showing the bending of CNTs due to surface relief of the S/D contacts. (inset) Schematic illustration of the top-gate/bottom-contact device structure with raised S/D electrodes.

Recent studies have shown that adequate top dielectric capping such as Al_2O_3 on SWCNTs leads to the observation of intrinsic ambipolar characteristics of SWCNT FETs by preventing the absorption of oxygen and water molecules [16, 73-75]. However, our short channel top-gate devices exhibit only slight ambipolarity even with a 30 nm thick Al_2O_3 top dielectric on the SWCNTs, which may be attributed to the bending of SWCNTs. In order to investigate the effect of bending of SWCNT, we fabricated top-gate/bottom-contact device with recessed S/D electrodes to minimize the bending of SWCNTs due to contact relief.

4.3.2. Short channel SWCNT FETs with recessed S/D electrodes

The device with recessed S/D electrodes was fabricated on a 270nm thick SiO_2 layer thermally grown on a heavily doped Si substrate. S/D electrodes with rectangular perimeters for inkjet printing were patterned on PMMA by EBL process followed by a dry etching step with CHF_3 plasma to form a 15 nm deep trench for the recessing of S/D electrodes. A bilayer of Ti/Pd (3 nm/13 nm) was deposited into the trench, followed by a lift-off process. A comparison of the device configurations and surface profiles between raised S/D electrodes and recessed S/D electrodes are shown in Figure 4.2.

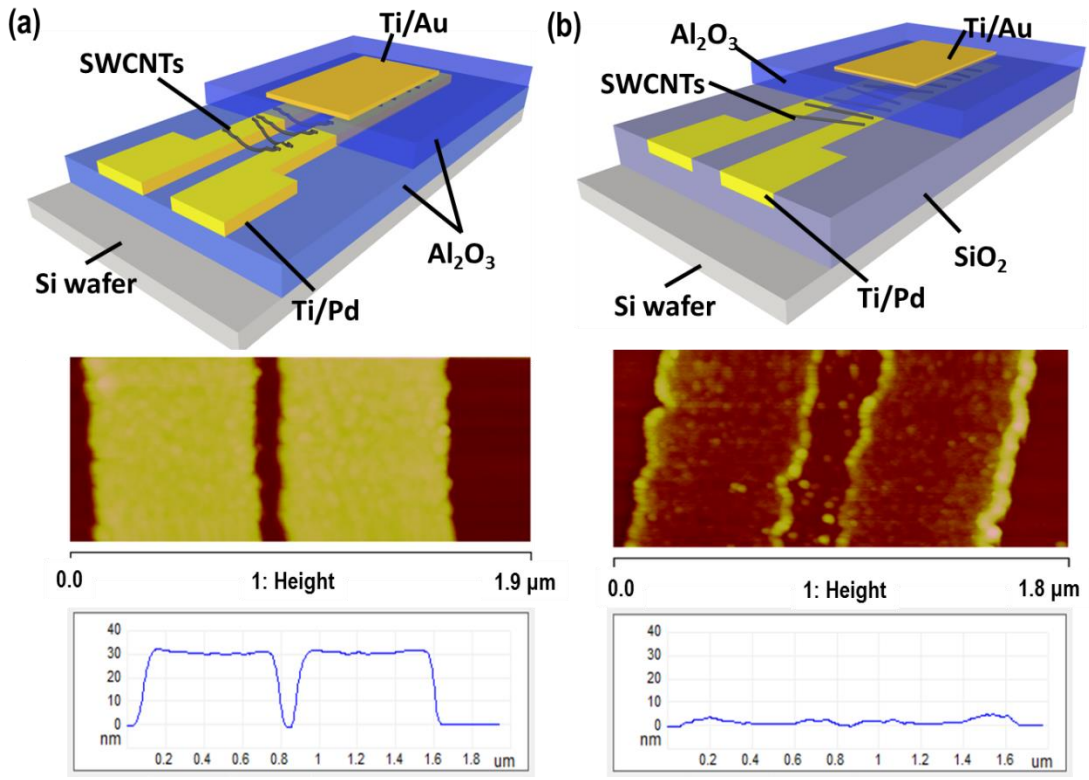

Figure 4.2: (a) A schematic illustration of a completed device of top-gate/bottom-contact structure with typical raised S/D electrodes. AFM image and step profile of stacked S/D electrodes. (b) A schematic illustration of a completed device of top-gate/bottom-contact structure with flattened S/D electrodes. AFM image and step profile of flattened S/D electrodes.

As shown in atomic force microscope (AFM) images in Figure 4.2, the height difference between S/D electrodes and SiO_2 surface of raised S/D and recessed S/D are ~30 nm and ~2 nm, respectively.

After depositing S/D electrodes, a single drop of high purity semiconducting SWCNT ink (0.05 mg/mL containing 0.5 pg of SWCNT) was printed on the prepatterned S/D area and the droplet was confined by rectangular perimeter forming an active layer. Following this step, a top dielectric of 30nm thick Al_2O_3 was deposited by atomic layer deposition (ALD) and the top gate electrode, a bilayer of Ti/Au (5 nm/35 nm), was patterned by EBL and completed via a lift-off process.

4.3.3. Electrical characteristics of short channel ambipolar SWCNT FETs

The electrical characteristics of inkjet printed SWCNT FETs with recessed S/D electrodes in top-gate/bottom-contact device structure are shown in Figure 4.3.

By employing recessed S/D electrodes, the degree of SWCNT bending was minimized resulting in balanced ambipolar characteristics, as shown in Figure 4.3 (a). A SWCNT FET with 10 SWCNTs as the active channel material (L_{ch} = 200 nm) shows I_{on}/I_{off} of ~10^3 (8.06×10^3 at V_{DS} = -0.5 V and 4.28×10^3 at V_{DS} = -1 V). Normalized by the number of SWCNTs in the channel, transconductance (g_m) values exceed 0.1 μS/tube at V_{DS} = -1V.

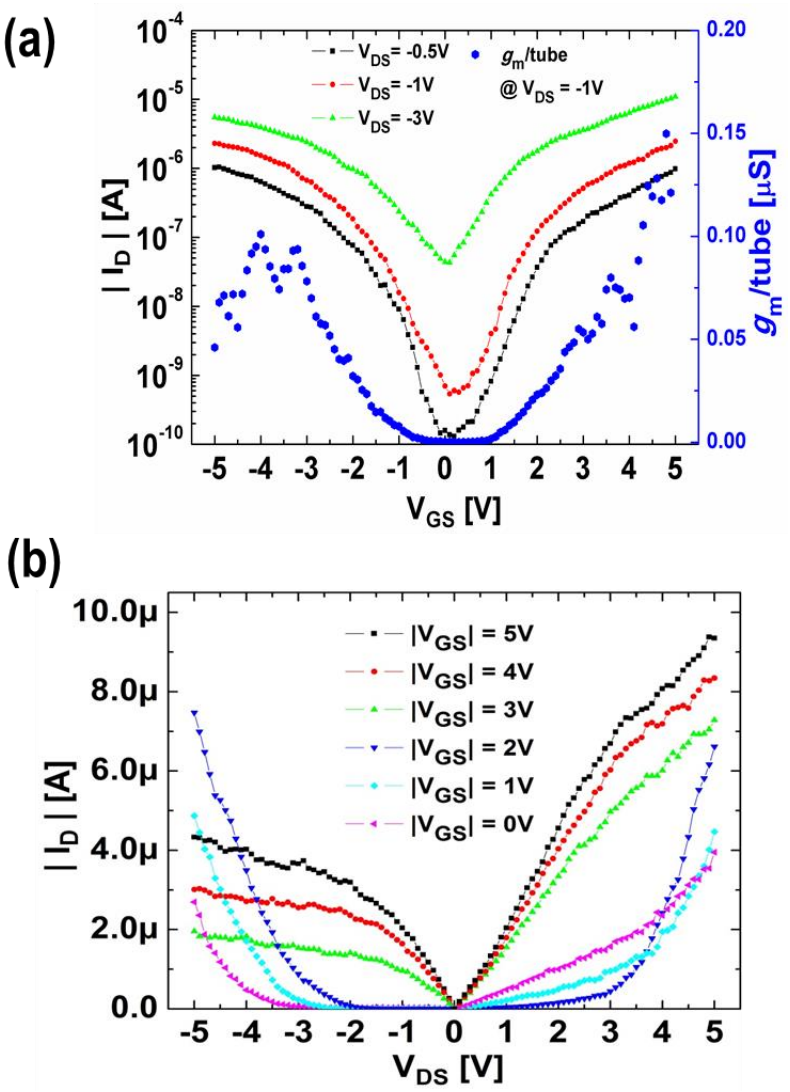

Figure 4.3: Electrical characteristics of top-gate/bottom-contact device with flattened S/D electrodes. (a) I_D-V_G transfer characteristics of device with channel length 200nm showing balanced ambipolar characteristic with 10 SWCNTs (blue hexagons are transconductance per SWCNT). (b) I_D-V_D output characteristics of device with channel length of 200nm.

As shown in Figure 4.4 (a), top-gate/bottom-contact devices with recessed S/D electrodes are substantially stable in air. Moreover, top-gate/bottom-contact device with

recessed S/D electrodes shows a robust shelf life up to 6 months as illustrated in Figure 4.4 (b).

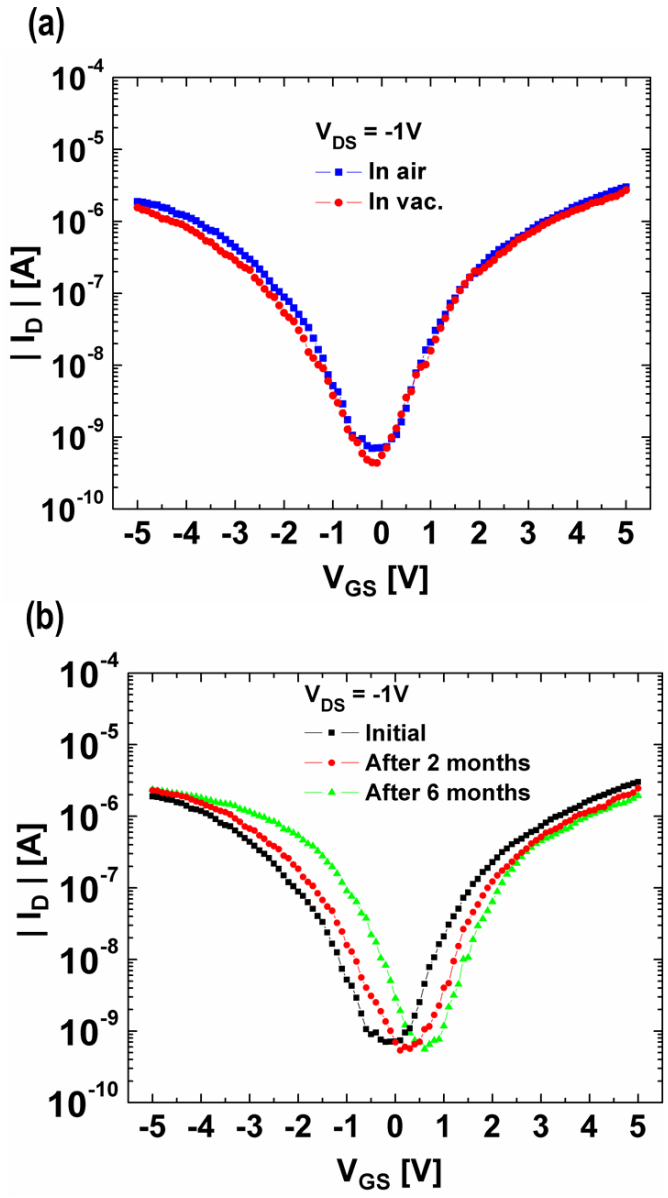

Figure 4.4: (a) Comparison of I_D-V_G transfer characteristics between measurments in air and vacuum (1×10^{-3} Torr) for a top-gate/bottom contact device with recessed S/D electrodes. (b) Shelf life of a top-gate/bottom contact device with recessed S/D electrodes stored in air.

4.3.4. Gate insulator interface modification by fluoropolymer

Deposition of fluoropolymer, P(VDF-TrFE), on networked SWCNTs can enhance the p-channel behavior of SWCNT device performance as reported in our previous work [43]. In the top-gate/bottom-contact device structure with recessed S/D electrodes, a single droplet (10 pL) of P(VDF-TrFE) was inkjet printed on SWCNTs prior to the top dielectric deposition process. This simple inkjet printing of P(VDF-TrFE) can selectively convert the polarity of the device to p-type as shown in Figure 4.5. A thin P(VDF-TrFE) (<5nm) layer inkjet printed onto SWCNTs on flat S/D electrodes enhances the hole transport and reduces the effect of Al_2O_3 capping, resulting in p-type doping (see Figure 4.5 (a)). Figure 4.5 (b) shows statistical data of 3 types of device structures (10 devices for each structure): conventional top-gate/bottom-contact structure, recessed S/D electrode devices, and P(VDF-TrFE) on recessed S/D electrode devices investigated in this work. ON-current values of the p-branch and n-branch were extracted from 30 devices and bias conditions were at V_{GS} = -3 V, V_{GS} = 3 V, respectively.

The data clearly show that the inclusion of the interfacial P(VDF-TrFE) layer leads to enhanced hole concentrations and a shifted threshold voltage that favors p-channel operation. Additionally, in some of the devices, the n-channel mobility was reduced. Thus, deposition of a thin interfacial P(VDF-TrFE) layer between the SWCNTs and the Al_2O_3 gate insulator is a reproducible way to suppress ambipolar behavior resulting in dominantly p-channel devices. This will be beneficial in the construction of logic circuits where the use of only ambipolar components leads to higher power dissipation [54, 76]. As recently shown, logic circuits with p-channel along with ambipolar components possess higher performance than circuits with p-channel only devices in terms of power dissipation and noise margin [77].

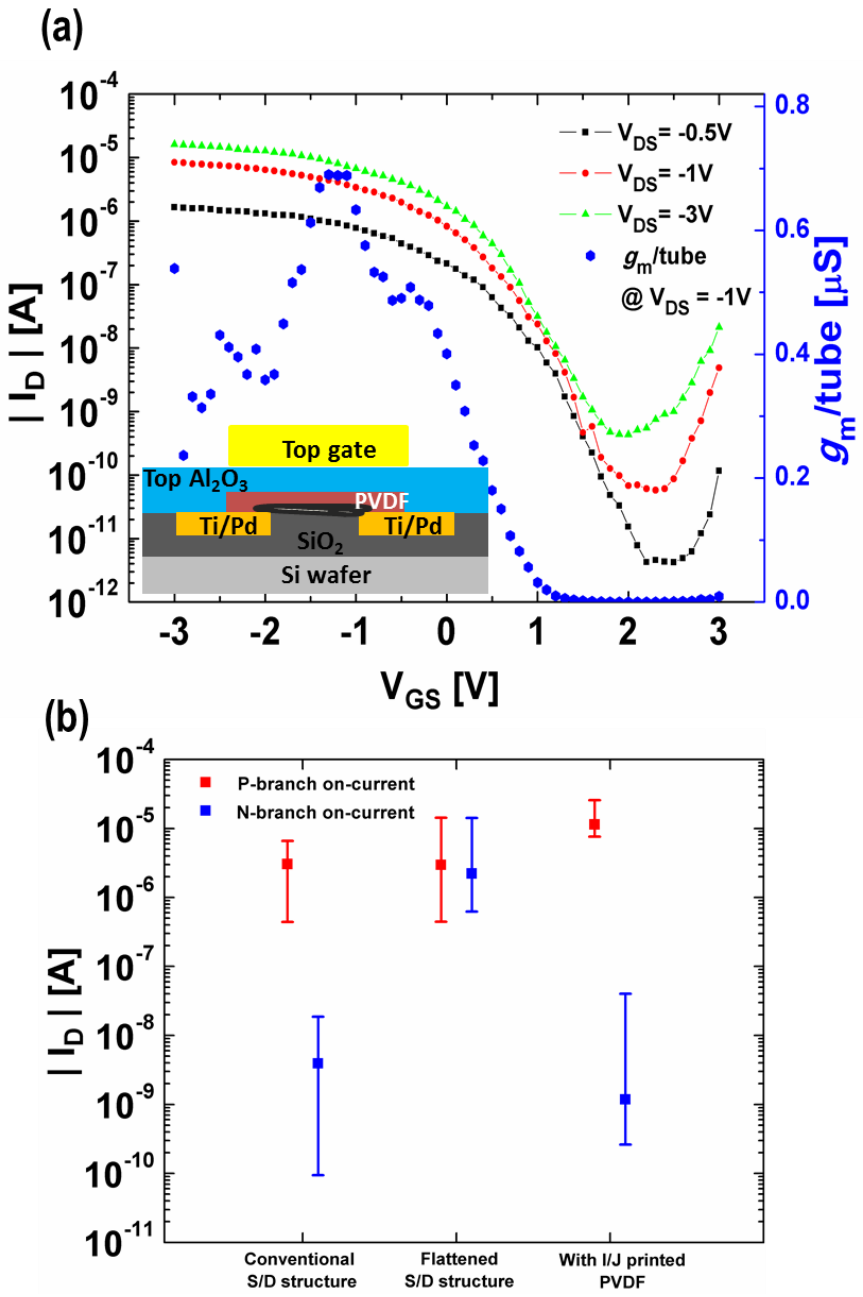

Figure 4.5: (a) Electrical characteristics of a top-gate/bottom contact device with flattened S/D electrodes and inkjet printed P(VDF-TrFE) (L_{ch} = 200 nm). (b) Statistical data of the p-branch and n-branch on-current levels for various device structures (10 devices for each structure).

4.4 CONCLUSION

In conclusion, we have demonstrated short channel ambipolar FETs with inkjet printed semiconducting SWCNTs by employing a recessed S/D electrode structure in top-gate/bottom-contact device configuration. Loss of ambipolar behavior, resulting in dominantly p-channel behavior, can be reproducibly achieved through two mechanisms: (i) mechanical distortion of the nanotubes by surface relief at the edge of raised source and drain contacts and (ii) inclusion of a very thin interfacial layer of P(VDF-TrFE) between the SWCNT layer and the Al_2O_3 top gate insulator. The use of P(VDF-TrFE) will be a useful way to realize p-channel SWCNT FET devices, which are required for some circuit design applications.

Chapter 5. Conclusion

In this dissertation, various inkjet printed single-walled carbon nanotube (SWCNT) transistors were demonstrated: from nano-scale short channel devices to conventional micron-scale channel length devices.

In conventional inkjet printed SWCNT devices, in which the channel length is micron-scale, we have shown that the use of coatings of the fluoropolymer containing copolymer P(VDF-TrFE) results in substantial improvements in the characteristics of SWCNT FET devices and circuits comprised of these devices. At the device level, there is a significant decrease in the following: (a) Off-current magnitude; (b) Degree of hysteresis; (c) Variation in threshold voltage; and (d) Bias stress degradation. We attribute this to the effects of oriented polar C-F bonds in the P(VDF-TrFE) which partially neutralize charges impurities and defects in the semiconductor and the semiconductor-gate insulator interface. Experiments investigating the effects of polar vapors on device characteristics support this model. At the circuit level, the improved uniformity in device characteristics plus the effects listed above, result in improved performance of 5-stage complementary ring oscillator circuits. The use of such capping layers will be greatly beneficial to the adoption of SWCNT based circuits for a variety of applications.

We have also demonstrated a method of inkjet printing submicron-scale SWCNT FETs with channel lengths of 150 nm - 250 nm, far less than the average length of SWCNTs (1.36 μm). In addition, the transistor electrode design implies minimal consumption of SWCNT ink (a single droplet of 10 pL ink containing 0.5 pg of SWCNTs), thus realizing one of the primary benefits of additive manufacturing. The transconductance and mobility values of these short channel devices greatly exceed those

of previously reported inkjet printed SWCNT FETs, with the added benefit of roll-to-roll compatibility. We compared the fabrication process and characteristics of SWCNT FETs employing two different device structures, bottom-gate/top-contact and top-gate/bottom-contact, and found the top-gate/bottom-contact device to possess distinct advantages from both processing and performance perspectives. Overall, this work will impact ongoing efforts to realize high-performance electronic devices in a manner compatible with roll-to-roll additive manufacturing methods.

Short channel ambipolar FETs with inkjet printed semiconducting SWCNTs by employing a recessed S/D electrode structure in top-gate/bottom-contact device configuration were demonstrated. Loss of intrinsic ambipolar behavior in top-gate/bottom-contact structure, resulting in dominantly p-channel behavior, can be reproducibly achieved through two mechanisms: (i) mechanical distortion of the nanotubes by surface relief at the edge of raised source and drain contacts and (ii) inclusion of a very thin interfacial layer of P(VDF-TrFE) between the SWCNT layer and the Al_2O_3 top gate insulator. The use of P(VDF-TrFE) will be a useful way to realize p-channel SWCNT FET devices, which are required for some circuit design applications.

For future work, roll-to-roll printing technologies, such as nanoimprint lithography can be combined with our inkjet printing process. Since similar source/drain spacing used in our short channel devices can be realized by nanoimprint lithography, various short channel SWCNT FETs and circuits can be fabricated using roll-to-roll printing even on the flexible substrates. By employing other capping layers which enable n-type operation with recessed S/D structure, complementary circuits can be realized with inkjet printed SWCNTs and P(VDF-TrFE). Based on the inkjet printed short channel SWCNT FET, printed electronics that require high-speed performance such as rectifiers can be implemented.

Appendix

List of Publications

1. **S. Jang**, S. Kim, M. L. Geier, M. C. Hersam, and A. Dodabalapur, "Inkjet Printed Carbon Nanotubes in Short Channel Field Effect Transistors: Influence of Nanotube Distortion and Gate Insulator Interface Modification," *Flexible and Printed Electronics,* Under review
2. **S. Jang**, B. Kim, M. L. Geier, M. C. Hersam, A. Dodabalapur, "Short channel Field Effect Transistors with Inkjet Printed Semiconducting Carbon Nanotubes", *Small*, Vol. 11, No 41, 5505 (2015) (+**Journal Front Cover**)
3. **S. Jang**, B. Kim, M. L. Geier, P. L. Prabhumirashi, M. C. Hersam, A. Dodabalapur, "Fluoropolymer coatings for improved carbon nanotube transistor device and circuit performance", *Applied Physics Letters*, Vol. 105, 122107 (2014) **(+AIP press released)**
4. B. Kim, **S. Jang**, M. L. Geier, P. L. Prabhumirashi, M. C. Hersam, A. Dodabalapur, "High-Speed, Inkjet-Printed Carbon Nanotube/Zinc Tin Oxide Hybrid Complementary Ring Oscillators", *Nano Letters*, Vol. 14, 3683 (2014)
5. B. Kim, **S. Jang**, M. L. Geier, P. L. Prabhumirashi, M. C. Hersam, A. Dodabalapur, "Inkjet Printed Ambipolar Transistors and Inverters Based on Carbon Nanotube/Zinc Tin Oxide Heterostructures", *Applied Physics Letters*, Vol. 104, 062101 (2014)
6. B. Kim, **S. Jang**, P. L. Prabhumirashi, M. L. Geier, M. C. Hersam, A. Dodabalapur, "Low Voltage, High Performance Inkjet Printed Carbon Nanotube Transistors with Solution Processed ZrO_2 Gate Insulator", *Applied Physics Letters*, Vol. 103, 082119 (2013)
7. **S. Jang,** B. Kim, L. Schulz, L. Wang, B. Cobb, A. Dodabalapur "Scaling Effects in Organic, Amorphous Oxide, and Printed Single Walled Carbon Nanotube Thin-Film Transistors", *International Thin-Film Transistor Conference (ITC 2016)*, Hsinchu, Taiwan (2016) *(Invited)*
8. **S. Jang**, B. Kim, M. L. Geier, M. C. Hersam, A. Dodabalapur "Defect Screening Effects of Fluoropolymer Capping in Single Walled Carbon Nanotube Transistors", *American Physical Society March Meeting (APS March Meeting)*, B17.00010, San Antonio, TX, U.S. (2015)
9. **S. Jang**, B. Kim, M. L. Geier, M. C. Hersam, A. Dodabalapur "Short Channel Ambipolar Transistors with Inkjet Printed Semiconducting Single Walled Carbon Nanotube", *Material Research Society Spring Meeting (MRS Spring)*, T13.09, San Francisco, CA, U.S. (2015)

10. **S. Jang**, B. Kim, Seohee Kim, Taejun Ha, Chenguan Lee, A. Dodabalapur "Comparison of polymer, carbon nanotube and amorphous metal oxide TFTs for printable electronics", *International Workshop on Flexible & Printable Electronics (IWFPE)*, Jeonju, Republic of Korea (2014) *(Invited)*
11. **S. Jang**, B. Kim, M. L. Geier, P. L. Prabhumirashi, M. C. Hersam, A. Dodabalapur "Inkjet Printed Nano-scale Carbon Nanotube Transistors", *Material Research Society Spring Meeting (MRS Spring)*, MM9.04, San Francisco, CA, U.S. (2014)
12. **S. Jang**, B. Kim, M. L. Geier, P. L. Prabhumirashi, M. C. Hersam, A. Dodabalapur "Nano-Scaled Carbon Nanotube Transistors Fabricated by Inkjet Printing", *Material Research Society Fall Meeting (MRS Fall)*, SS19.109, Boston, MA, U.S. (2013)

References

[1] A. Dodabalapur, "Organic and polymer transistors for electronics," *Mater. Today,* vol. 9, pp. 24-30, 2006.

[2] P. Sonar, S. P. Singh, Y. Li, M. S. Soh, and A. Dodabalapur, "A Low-Bandgap Diketopyrrolopyrrole-Benzothiadiazole-Based Copolymer for High-Mobility Ambipolar Organic Thin-Film Transistors," *Adv. Mater.,* vol. 22, pp. 5409-5413, 2010.

[3] A. Teichler, J. Perelaer, and U. S. Schubert, "Inkjet printing of organic electronics – comparison of deposition techniques and state-of-the-art developments," *J. Mater. Chem. C,* vol. 1, p. 16, 2013.

[4] S. Chung, J. Jang, J. Cho, C. Lee, S.-K. Kwon, and Y. Hong, "All-Inkjet-Printed Organic Thin-Film Transistors with Silver Gate, Source/Drain Electrodes," *Jpn. J. Appl. Phys.,* vol. 50, p. 5, 2011.

[5] T. H. Lee, B. Lüssem, K. Kim, G. Giri, Y. Nishi, and Z. Bao, "p-Channel Field-Effect Transistors Based on C60 Doped with Molybdenum Trioxide," *ACS Appl. Mater. Interfaces,* vol. 5, pp. 2337-2341, 2013/04/10 2013.

[6] P. Avouris, Z. Chen, and V. Perebeinos, "Carbon-based electronics," *Nat. Nanotechnol.,* vol. 2, p. 11, 2007.

[7] S.-J. Choi, P. Bennett, K. Takei, ChuanWang, C. C. Lo, A. Javey*, et al.*, "Short-Channel Transistors Constructed with Solution-Processed Carbon Nanotubes," *ACS Nano,* vol. 7, p. 6, 2013.

[8] D. Shahrjerdi, A. D. Franklin, S. Oida, J. A. Ott, G. S. Tulevski, and W. Haensch, "High Performance Air-Stable n-Type Carbon Nanotube Transistors with Erbium Contacts," *ACS Nano,* vol. 7, p. 6, 2013.

[9] A. D. Franklin, G. S. Tulevski, S.-J. Han, D. Shahrjerdi, Q. Cao, H.-Y. Chen*, et al.*, "Variability in Carbon Nanotube Transistors: Improving Device-to-Device Consistency," *ACS Nano,* vol. 6, pp. 1109-1115, 2012/02/28 2012.

[10] C. Wang, K. Takei, T. Takahashi, and A. Javey, "Carbon nanotube electronics--moving forward," *Chem. Soc. Rev.,* vol. 42, pp. 2592-609, Apr 7 2013.

[11] D.-H. Lee, S.-Y. Han, G. S. Herman, and C.-h. Chang, "Inkjet printed high-mobility indium zinc tin oxide thin film transistors," *J. Mater. Chem.,* vol. 19, p. 3135, 2009.

[12] P. K. Nayak, M. N. Hedhili, D. Cha, and H. N. Alshareef, "Impact of Soft Annealing on the Performance of Solution-Processed Amorphous Zinc Tin Oxide Thin-Film Transistors," *ACS Appl. Mater. Interfaces,* vol. 5, pp. 3587-3590, 2013/05/08 2013.

[13] K. Everaerts, L. Zeng, J. W. Hennek, D. I. Camacho, D. Jariwala, M. J. Bedzyk, *et al.*, "Printed Indium Gallium Zinc Oxide Transistors. Self-Assembled Nanodielectric Effects on Low-Temperature Combustion Growth and Carrier Mobility," *ACS Appl. Mater. Interfaces,* vol. 5, pp. 11884-11893, 2013/11/27 2013.

[14] F. S. Kim, E. Ahmed, S. Subramaniyan, and S. A. Jenekhe, "Air-Stable Ambipolar Field-Effect Transistors and Complementary Logic Circuits from Solution-Processed n/p Polymer Heterojunctions," *ACS Appl. Mater. Interfaces,* vol. 2, pp. 2974-2977, 2010/11/24 2010.

[15] T. N. Ng, B. Russo, B. Krusor, R. Kist, and A. C. Arias, "Organic inkjet-patterned memory array based on ferroelectric field-effect transistors," *Organic Electronics,* vol. 12, pp. 2012-2018, 2011.

[16] M. Ha, J. W. Seo, P. L. Prabhumirashi, W. Zhang, M. L. Geier, M. J. Renn, *et al.*, "Aerosol jet printed, low voltage, electrolyte gated carbon nanotube ring oscillators with sub-5 mus stage delays," *Nano Lett.,* vol. 13, pp. 954-60, Mar 13 2013.

[17] C. Wang, J. C. Chien, K. Takei, T. Takahashi, J. Nah, A. M. Niknejad, *et al.*, "Extremely bendable, high-performance integrated circuits using semiconducting carbon nanotube networks for digital, analog, and radio-frequency applications," *Nano Lett.,* vol. 12, pp. 1527-33, Mar 14 2012.

[18] Y. Nobusa, Y. Yomogida, S. Matsuzaki, K. Yanagi, H. Kataura, and T. Takenobu, "Inkjet printing of single-walled carbon nanotube thin-film transistors patterned by surface modification," *Appl. Phys. Lett.,* vol. 99, p. 183106, 2011.

[19] M. Steiner, M. Engel, Y.-M. Lin, Y. Wu, K. Jenkins, D. B. Farmer, *et al.*, "High-frequency performance of scaled carbon nanotube array field-effect transistors," *Appl. Phy. Lett.,* vol. 101, p. 053123, 2012.

[20] Y. Liu, Z. Jin, J. Wang, R. Cui, H. Sun, F. Peng, *et al.*, "Nitrogen-Doped Single-Walled Carbon Nanotubes Grown on Substrates: Evidence for Framework Doping and Their Enhanced Properties," *Adv. Funct. Mater.,* vol. 21, pp. 986-992, 2011.

[21] M. S. Arnold, A. A. Green, J. F. Hulvat, S. I. Stupp, and M. C. Hersam, "Sorting carbon nanotubes by electronic structure using density differentiation," *Nat. Nanotechnol.,* vol. 1, pp. 60-5, Oct 2006.

[22] A. A. Green and M. C. Hersam, "Nearly single-chirality single-walled carbon nanotubes produced via orthogonal iterative density gradient ultracentrifugation," *Adv. Mater.,* vol. 23, pp. 2185-90, May 17 2011.

[23] G. S. Tulevski, A. D. Franklin, and A. Afzali, "High Purity Isolation and Quantification of Semiconducting Carbon Nanotubes via Column Chromatography," *ACS Nano,* vol. 7, pp. 2971-2976, 2013/04/23 2013.

[24] P. H. Lau, K. Takei, C. Wang, Y. Ju, J. Kim, Z. Yu, *et al.*, "Fully printed, high performance carbon nanotube thin-film transistors on flexible substrates," *Nano Lett.,* vol. 13, pp. 3864-9, Aug 14 2013.

[25] J. Minhun, K. Jaeyoung, N. Jinsoo, L. Namsoo, L. Chaemin, L. Gwangyong, *et al.*, "All-Printed and Roll-to-Roll-Printable 13.56-MHz-Operated 1-bit RF Tag on Plastic Foils," *IEEE Trans. on Electron Devices,,* vol. 57, pp. 571-580, 2010.

[26] D. Redinger, S. Molesa, S. Yin, R. Farschi, and V. Subramanian, "An Ink-Jet-Deposited Passive Component Process for RFID," *IEEE Trans. on Electron Devices,* vol. 51, p. 6, 2004.

[27] B. Kim, S. Jang, P. L. Prabhumirashi, M. L. Geier, M. C. Hersam, and A. Dodabalapur, "Low voltage, high performance inkjet printed carbon nanotube transistors with solution processed ZrO2 gate insulator," *Appl. Phy. Lett.,* vol. 103, p. 5, 2013.

[28] K. Heo, C.-J. Kim, M.-H. Jo, and S. Hong, "Massive integration of inorganic nanowire-based structures on solid substrates for device applications," *J. Mater. Chem.,* vol. 19, pp. 901-908, 2009.

[29] D. G. Bucknall, *Nanolithography and Patterning Techniques in Microelectronics*: Woodhead Pub., 2005.

[30] H. Kipphan, *Handbook of Print Media : Technologies and Production Methods*: Springer, 2001.

[31] A. pique and D. B. Chrisey, *Direct-write Technologies for Rapid Prototyping Applications*: Academic Press, 2002.

[32] B. Ballarin, A. Fraleoni-Morgera, D. Frascaro, S. Marazzita, C. Piana, and L. Setti, "Thermal inkjet microdeposition of PEDOT:PSS on ITO-coated glass and characterization of the obtained film," *Synthetic Metals,* vol. 146, pp. 201-205, 2004.

[33] FUJIFIRLM Dimatix. Inc., "FUJIFILM Dimatix Material Printer DMP-2800 Seriese User's Manual Version 2.0," ed: FUJIFILM Dimatix, Inc.

[34] D. B. Bogy and F. E. Taike, "Experimental and Theoretical Study of Wave Propagation Phenomena in Drop-on-Demand Ink Jet Devices," *IBM J. Res. Develop.,* vol. 28, p. 11, 1984.

[35] W. S. Wong, E. M. Chow, R. Lujan, V. Geluz-Aguilar, and M. L. Chabinyc, "Fine-feature patterning of self-aligned polymeric thin-film transistors fabricated by digital lithography and electroplating," *Appl. Phys. Lett.,* vol. 89, p. 142118, 2006.

[36] J. Vaillancourt, H. Zhang, P. Vasinajindakaw, H. Xia, X. Lu, X. Han, *et al.*, "All ink-jet-printed carbon nanotube thin-film transistor on a polyimide substrate with

an ultrahigh operating frequency of over 5 GHz," *Appl. Phys. Lett.,* vol. 93, p. 243301, 2008.

[37] S. Iijima and T. Ichihashi, "Single-shell carbon nanotubes of 1-nm diameter," *Nature,* vol. 363, p. 3, 1993.

[38] R. Saito, G. Dresselhaus, and M. S. Dresselhaus. *Physical Properties Of Carbon Nanotubes (1st ed.)*. : Singapore, World Science Publishing company, 1998 Available: http://UTXA.eblib.com/patron/FullRecord.aspx?p=183760

[39] M. S. Arnold, S. I. Stupp, and M. C. Hersam, "Enrichment of Single-Walled Carbon Nanotubes by Diameter in Density Gradients," *Nano Lett.,* vol. 5, pp. 713-718, 2005.

[40] FUJIFIRLM Dimatix. Inc., "FUJIFILM Dimatix Ink Tutorial," ed: FUJIFILM Dimatix Inc.

[41] J. Zhao, Y. Gao, W. Gu, C. Wang, J. Lin, Z. Chen*, et al.*, "Fabrication and electrical properties of all-printed carbon nanotube thin film transistors on flexible substrates," *J. Mater. Chem.,* vol. 22, p. 20747, 2012.

[42] S. D. Bergin, Z. Sun, D. Rickard, P. V. Streich, J. P. Hamilton, and J. N. Coleman, "Multicomponent Solubility Parameters for Single-Walled Carbon Nanotube-Solvent Mixtures," *ACS Nano,* vol. 3, p. 11, 2009.

[43] S. Jang, B. Kim, M. L. Geier, P. L. Prabhumirashi, M. C. Hersam, and A. Dodabalapur, "Fluoropolymer coatings for improved carbon nanotube transistor device and circuit performance," *Appl. Phys. Lett.,* vol. 105, p. 122107, 2014.

[44] S. Jang, B. Kim, M. L. Geier, M. C. Hersam, and A. Dodabalapur, "Short Channel Field-Effect-Transistors with Inkjet-Printed Semiconducting Carbon Nanotubes," *Small,* vol. 11, pp. 5505-5509, 2015.

[45] S. Jang, S. Kim, M. L. Geier, M. C. Hersam, and A. Dodabalapur, "Inkjet Printed Carbon Nanotubes in Short Channel Field Effect Transistors: Influence of Nanotube Distortion and Gate Insulator Interface Modification," *Flexible and Printed Electronics,* 2016.

[46] R. Martel, V. Derycke, C. Lavoie, J. Appenzeller, K. K. Chan, J. Tersoff*, et al.*, "Ambipolar Electrical Transport in Semiconducting Single-Wall Carbon Nanotubes," *Phys. Rev. Lett.,* vol. 87, p. 256805, 2001.

[47] Y.-M. Lin, J. Appenzeller, and P. Avouris, "Ambipolar-to-Unipolar Conversion of Carbon Nanotube Transistors by Gate Structure Engineering," *Nano Lett.,* vol. 4, pp. 947-950, 2004/05/01 2004.

[48] Y.-M. Lin, J. Appenzeller, J. Knoch, and P. Avouris, "High-Performance Carbon Nanotube Field-Effect Transistor With Tunable Polarities," *IEEE Trans. Nanotechnol.,* vol. 4, p. 9, 2005.

[49] V. Derycke, R. Martel, J. Appenzeller, and P. Avouris, "Controlling doping and carrier injection in carbon nanotube transistors," *Appl. Phys. Lett.,* vol. 80, pp. 2773-2775, 2002.

[50] A. Lin, N. Patil, K. Ryu, A. Badmaev, L. G. De Arco, Z. Chongwu*, et al.*, "Threshold Voltage and On-Off Ratio Tuning for Multiple-Tube Carbon Nanotube FETs," *IEEE Trans. Nanotechnol.,* vol. 8, pp. 4-9, 2009.

[51] T.-J. Ha, J. Lee, S. F. Chowdhury, D. Akinwande, P. J. Rossky, and A. Dodabalapur, "Transformation of the Electrical Characteristics of Graphene Field-Effect Transistors with Fluoropolymer," *ACS Appl. Mater. Interfaces,* vol. 5, pp. 16-20, 2013.

[52] D. R. Lide, *Handbook of Organic Solvents*., Boca Raton, FL: CRC Press, 1994.

[53] J. A. Riddick, W. B. Bunger, and T. K. Sakano, *Organic Solvents*, Forth ed., New York: John Wiley & Sons, 1986.

[54] B. Kim, S. Jang, M. L. Geier, P. L. Prabhumirashi, M. C. Hersam, and A. Dodabalapur, "High-Speed, Inkjet-Printed Carbon Nanotube/Zinc Tin Oxide Hybrid Complementary Ring Oscillators," *Nano Lett.,* vol. 14, p. 5, 2014.

[55] A. D. Franklin, M. Luisier, S. J. Han, G. Tulevski, C. M. Breslin, L. Gignac*, et al.*, "Sub-10 nm carbon nanotube transistor," *Nano Lett.,* vol. 12, pp. 758-62, Feb 8 2012.

[56] V. K. Sangwan, R. P. Ortiz, J. M. P. Alaboson, J. D. Emery, M. J. Bedzyk, L. J. Lauhon*, et al.*, "Fundamental Performance Limits of Carbon Nanotube Thin-Film Transistors Achieved Using Hybrid Molecular Dielectrics," *ACS Nano,* vol. 6, p. 9, 2012.

[57] S. H. Ahn, S. Yang, M. Miller, M. Ganapathisubramanian, M. Menezes, J. Choi*, et al.*, "High-performance wire-grid polarizers using jet and Flash™ imprint lithography," *Journal of Micro/Nanolithography, MEMS, and MOEMS,* vol. 12, pp. 031104-031104, 2013.

[58] J. G. Ok, S. H. Ahn, M. K. Kwak, and L. J. Guo, "Continuous and high-throughput nanopatterning methodologies based on mechanical deformation," *J. Mater. Chem. C,* vol. 1, pp. 7681-7691, 2013.

[59] C. J. V. OSS, M. K. CHAUDHURY, and R. J. GOOD, "Interfacial Lifshitz-van der Waals and Polar Interactions in Macroscopic Systems," *Chem. Rev.,* vol. 88, p. 15, 1988.

[60] F. K. Hansen, "The Measurement of Surface Energy of Polymers by Means of Contact Angles of Liquids on Solid Surfaces," *University of Oslo,* 2004.

[61] A. Setiadi, M. Akai-Kasaya, A. Saito, and Y. Kuwahara, "Advantages of flattened electrode in bottom contact single-walled carbon nanotube field-effect transistor," *Appl. Phys. Lett.,* vol. 105, p. 093506, 2014.

[62] S. Suzuki, K. Kanzaki, Y. Homma, and S.-y. Fukuba, "Low-Acceleration-Voltage Electron Irradiation Damage in Single-Walled Carbon Nanotubes," *Jpn. J. Appl. Phys.,* vol. 43, p. L1118, 2004.

[63] S. K. Pillai and M. B. Chan-Park, "High-performance printed carbon nanotube thin-film transistors array fabricated by a nonlithography technique using hafnium oxide passivation layer and mask," *ACS Appl. Mater. Interfaces,* vol. 4, pp. 7047-54, Dec 2012.

[64] C. W. Lee, S. K. Raman Pillai, X. Luan, Y. Wang, C. M. Li, and M. B. Chan-Park, "High-performance inkjet printed carbon nanotube thin film transistors with high-k HfO2 dielectric on plastic substrate," *Small,* vol. 8, pp. 2941-7, Oct 8 2012.

[65] H. Okimoto, T. Takenobu, K. Yanagi, Y. Miyata, H. Shimotani, H. Kataura*, et al.*, "Tunable Carbon Nanotube Thin-Film Transistors Produced Exclusively via Inkjet Printing," *Adv. Mater.,* vol. 22, pp. 3981-3986, 2010.

[66] S.-J. Han, S. Oida, H. Park, J. B. Hannon, G. S. Tulevski, and W. Haensch, "Carbon Nanotube complementary logic based on Erbium contacts and self-assembled high purity solution tubes," *IEDM Tech. Dig.,* vol. 515, p. 4, 2013.

[67] M. L. Geier, J. J. McMorrow, W. Xu, J. Zhu, C. H. Kim, T. J. Marks*, et al.*, "Solution-processed carbon nanotube thin-film complementary static random access memory," *Nat. Nanotechnol.,* vol. 10, pp. 944-948, 11//print 2015.

[68] A. D. Franklin, D. B. Farmer, and W. Haensch, "Defining and Overcoming the Contact Resistance Challenge in Scaled Carbon Nanotube Transistors," *ACS Nano,* vol. 8, pp. 7333-7339, 2014/07/22 2014.

[69] H. Wei, M. Shulaker, H.-S. P. Wong, and S. Mitra, "Monolithic 3-dimensional intergration of CNT FET complimentary logic circuits," *IEDM Tech. Dig.,* vol. 511, p. 4, 2013.

[70] H. Wang, B. Cobb, A. van Breemen, G. Gelinck, and Z. Bao, "Highly Stable Carbon Nanotube Top-Gate Transistors with Tunable Threshold Voltage," *Adv. Mater.,* vol. 26, pp. 4588-4593, 2014.

[71] Y. Chai, A. Hazeghi, K. Takei, H.-Y. Chen, P. C. H. Chan, A. Javey*, et al.*, "Low-Resistance Electrical Contact to Carbon NanotubesWith Graphitic Interfacial Layer," *IEEE Trans. Electron Dev.,* vol. 59, p. 8, 2012.

[72] Y. Okuno, Y. Saito, S. Kawata, and P. Verma, "Tip-Enhanced Raman Investigation of Extremely Localized Semiconductor-to-Metal Transition of a Carbon Nanotube," *Phys. Rev. Lett.,* vol. 111, p. 216101, 2013.

[73] Y. Che, H. Chen, H. Gui, J. Liu, B. Liu, and C. Zhou, "Review of carbon nanotube nanoelectronics and macroelectronics," *Semicond. Sci. Technol.,* vol. 29, p. 073001, 2014.

[74] B. Kim, M. L. Geier, M. C. Hersam, and A. Dodabalapur, "Inkjet Printed Circuits on Flexible and Rigid Substrates Based on Ambipolar Carbon Nanotubes with High Operational Stability," *ACS Appl. Mater.Interfaces,* vol. 7, pp. 27654-27660, 2015/12/23 2015.

[75] J. Zhang, C. Wang, Y. Fu, Y. Che, and C. Zhou, "Air-Stable Conversion of Separated Carbon Nanotube Thin-Film Transistors from p-Type to n-Type Using Atomic Layer Deposition of High-κ Oxide and Its Application in CMOS Logic Circuits," *ACS Nano,* vol. 5, pp. 3284-3292, 2011/04/26 2011.

[76] B. Kim, S. Jang, M. L. Geier, P. L. Prabhumirashi, M. C. Hersam, and A. Dodabalapur, "Inkjet printed ambipolar transistors and inverters based on carbon nanotube/zinc tin oxide heterostructures," *Appl. Phys. Lett.,* vol. 104, pp. 062101, 2014.

[77] W. Xu, J. Dou, J. Zhao, H. Tan, J. Ye, M. Tange*, et al.*, "Printed thin film transistors and CMOS inverters based on semiconducting carbon nanotube ink purified by a nonlinear conjugated copolymer," *Nanoscale,* vol. 8, pp. 4588-4598, 2016.

Vita

Seonpil Jang was born in Seoul, South Koea on August 16th 1977, the son of Goonho Jang and Heeyoung Yang. He attended the Young-hoon High School, from which he graduated in 1996. He attended Hongik University in Seoul, South Korea, where he received a Bechelor of Engineering degree in Electronics and Electrical Engineering in 2004. He received Master of Science degree in Electrical, Information and Control Engineering from Hongik University, Seoul, South Korea in 2006. He was a research engineer at LCD R&D Center, Samsung Electronics from January 2006 to June 2011. He enrolled in The University of Texas at Austin in the fall of 2011 and began his study for Doctor of philosophy in Electrical and Computer Engineering. His doctoral research on inkjet printed carbon nanotube transistors was supervised by Professor Ananth Dodanalapur.

Permanent email address: ultratft@gmail.com

This dissertation was typed by Seonpil Jang.